PPPL-2158

DR-0655-6 I-18438

PPPL-2158

ANL/FPP-84-2

UC20-B

EXPERIMENTAL OBSERVATIONS OF THE COUPLING BETWEEN INDUCED CURRENTS AND MECHANICAL MOTION IN TORSIONALLY SUPPORTED SQUARE LOOPS AND PLATES

PART 1: EXPERIMENTAL ANALYSIS

By

D.W. Weissenburger, J.M. Bialek, G.J. Cargulia, M. Ulrickson
M.J. Knott, L. R. Turner, R.B. Wehrle

NOVEMBER 1984

PLASMA PHYSICS LABORATORY

PRINCETON UNIVERSITY

PRINCETON, NEW JERSEY

PREPARED FOR THE U.S. DEPARTMENT OF ENERGY,
UNDER CONTRACT DE-AC02-76-CHO-3073.

NOTICE

Printed in the United States of America

Available from:

National Technical Information Service
U.S. Department of Commerce
5285 Port Royal Road
Springfield, Virginia 22161

Price Printed Copy $ * ; Microfiche $4.50

*Pages	NTIS Selling Price
1-25	$7.00
25-50	$8.50
51-75	$10.00
76-100	$11.50
101-125	$13.00
126-150	$14.50
151-175	$16.00
176-200	$17.50
201-225	$19.00
226-250	$20.50
251-275	$22.00
276-300	$23.50
301-325	$25.00
326-350	$26.50
351-375	$28.00
376-400	$29.50
401-425	$31.00
426-450	$32.50
451-475	$34.00
476-500	$35.50
500-525	$37.00
526-550	$38.50
551-575	$40.00
567-600	$41.50

For documents over 600 pages, add $1.50 for each additional 25-page increment.

PPPL--2158

DE85 004401

EXPERIMENTAL OBSERVATIONS OF THE COUPLING BETWEEN INDUCED CURRENTS AND MECHANICAL MOTION IN TORSIONALLY SUPPORTED SQUARE LOOPS AND PLATES

PART 1: EXPERIMENTAL ANALYSIS

D. W. Weissenburger, J. M. Bialek, G. J. Cargulia, M. Ulrickson

Plasma Physics Laboratory, Princeton University

Princeton, NJ 08544, U.S.A.

M. J. Knott, L. R. Turner, R. B. Wehrle

Argonne National Laboratory

Argonne, IL 60439, U.S.A.

ABSTRACT

A series of experiments was successfully conducted to investigate the coupling between induced currents and rigid body rotation in square loops and plates. The experiments were performed with the Fusion Electromagnetic Induction Experiment (FELIX) facility at the Argonne National Laboratory. The observed data exhibited the magnetic damping and magnetic stiffness effects which arise in coupled systems and agreed very well with previous analytic calculations.

The experimental arrangement consisted of a conducting test piece which was rigidly mounted in a nonconducting fixture. The fixture was centered on a nonconducting axial tube which was constrained from rotation by adjustable leaf springs. The four examined test pieces were a copper loop, a bronze loop, a copper plate, and a stainless steel plate.

Electric currents were induced in a test piece by pulsing a vertical magnetic field. A constant horizontal magnetic field was also imposed during an experimental shot. The interaction of the induced currents and the magnetic fields produced a net torque about the fixture axis. Measurements were made of the total current flowing around the test piece and the angular rotation versus time.

The analysis of the experimental results and some representative data can be found in Part 1. A complete inventory of the data from the test shots as well as the predicted responses can be found in Part 2.

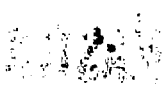

I. INTRODUCTION

This two-part report describes a series of experiments designed to provide quantitative data on coupled magnetomechanical systems. This first part presents the details of the data analysis, some representative data, the overall results, and conclusions. The second part[1] contains a complete inventory of all the test shots as well as the predicted responses.

In the next section a brief background is provided. This is followed by a section presenting the applicable differential equations for the experimental system. When the differential equations were simplified using small angle approximations, the resulting equations could be solved analytically. Within the bounds of the parameter space of the experiments, the analytic expressions generally proved to be very accurate predictors of the observed responses.

The fourth section describes the Fusion Electromagnetic Induction Experiment (FELIX) facility at the Argonne National Laboratory (ANL), where the experiments were performed, and the test fixture which was designed for this investigation.

The fifth section describes the static and dynamic mechanical tests which were performed with the test fixture and summarizes the results. Angular rotation versus time was measured using a rotational transducer attached to the fixture axis. These tests yielded the mechanical spring stiffness, moment of inertia, damping coefficient, and natural frequency.

The sixth section presents and summarizes the results of the tests which were made with the dipole field only, which produces no mechanical rotation. The total electric current flowing around a test piece was measured versus time using a Rogowski coil. These tests enabled us to refine our initial estimates of the dipole field magnitude and decay time constant.

The seventh section presents and summarizes the results of actual coupled tests which were made with both the dipole field and solenoid field. Both the test piece Rogowski coil and the rotational transducer were employed for these tests. The eighth section describes the second order effects which were observed in some of the tests and gives some possible sources. The ninth section summarizes the conclusions made from this series of experiments.

II. BACKGROUND

Electric currents may often be induced in conducting structures located close to magnetically confined fusion plasmas. These currents often interact with the background magnetic fields to produce significant mechanical forces. The rapid disappearance of plasma current during a plasma disruption is a particularly troublesome scenario. It became clear during the design of the Tokamak Fusion Test Reactor (TFTR) vacuum vessel internal hardware that an important coupling exists between the electrical and mechanical aspects of the analysis, which had not previously been investigated.

In a simple closed circuit, electromotive forces (emf's) are induced by varying magnetic fields according to Faraday's Law:

$$\varepsilon = - \frac{d\Phi}{dt} \tag{1}$$

where, $\varepsilon \equiv$ emf around the circuit (volts),

$\Phi \equiv$ magnetic flux through the circuit (webers)

$t \equiv$ time (seconds).

When the magnetic flux variation in a secondary circuit is produced by varying the current in a primary circuit, the induced emf in the secondary is called a transformer emf. When the magnetic flux variation in the secondary is produced by rigid body rotation or translation of the secondary circuit in a constant primary field, the induced emf in the secondary is called a motional emf. Induced emf's resulting from changing the shape of the secondary, deformational emf's, will not be addressed in this report. When currents are induced in extended conductors, i.e., plates or bodies instead of wires or coils, they are called eddy currents.

Initial analyses of TFTR components were made in an uncoupled fashion. Eddy currents were calculated using the computer code SPARK,[2] then the resulting loads were used as input for the structural analysis code MSC/NASTRAN.[3] SPARK calculates eddy currents using essentially only transformer emf's except that the external magnetic field drivers which produce the eddy currents may change in geometry as well as current. Driver geometries, however, are specified as input and are thus not the results of a coupled magnetomechanical analysis. Similarly, the NASTRAN computations did not attempt to include effects of motional emf's.

In regard to the vacuum vessel bumper limiter design for TFTR, the net mechanical response calculated by this uncoupled procedure produced relatively small structural displacements, but the corresponding velocities and accelerations were large. This observation led the Princeton Plasma Physics Laboratory (PPPL) to investigate and incorporate the coupled magnetomechanical effects into its analysis. This procedure and the application to the bumper limiter design were described by Bialek et al.[4] Related details on the bumper limiter were reported by Sevier et al.[5] A summary of the procedure follows.

The primary mode of mechanical vibration of the bumper limiter was similar to a rigid body rotation. The coupled equations for the rigid body rotation of a simply-supported rectangular loop were found to be amenable to solution both numerically and, when a small angle approximation was made, analytically. These equations are given in Sec. III.

The SPARK code was used to calculate the effective resistance, inductance, and area that should be used to approximate a rectangular plate with a rectangular loop. This was done by matching the total current flowing and net torque for a purely resistive distribution. The inductive time constant, L/R, was also matched to the observed primary time constant of the total current decaying by itself in the absence of external emf's. The resulting formulas are given in Sec. III.

The coupled solution obtained for the bumper limiter proved to be drastically different from the uncoupled solution for the expected plasma disruption scenario in TFTR. The next step was solving the mechanical equation by itself with the addition of an "equivalent mechanical damping"

term to account for the magnetic effects observed in the coupled solution. This technique provided an excellent match of the mechanical coupled solution for the parameter space of interest.

The final step was to include the "equivalent mechanical damping," calculated numerically from the coupled solution for the simply-supported model in the NASTRAN model of the bumper limiter. Actually, a conservative (low) estimate of the damping was used to account for the uncertainty involved in applying the results of the simple model to the detailed structural model.

The dramatic results obtained at PPPL inspired Turner and Cuthbertson[6] at ANL to investigate the simply-supported plate model by modifying the EDDYNET[7] computer code. The rigid body mechanical equation was solved simultaneously with the electric network mesh equations which were modified to include the motional emf's due to rotation. The ANL results corroborated the PPPL analyses. A joint effort between PPPL and ANL was instituted in early 1984 to test the basic predictions for the simply-supported loop and plate. PPPL specified and approved all designs made for the experiments. The fixture, test pieces, Rogowski coils, and all other hardware were fabricated by ANL. The test series was conducted during May of 1984.

III. MATHEMATICAL MODEL

The basic mathematical model employed in this analysis is essentially the same as that described in Ref. 4 except that we have included a mechanical damping term here. Figure 1 illustrates the basic model and the coordinate system used. The model consists of a rectangular loop or plate constrained on

a symmetry axis by a pair of rotational springs. A constant, spatially uniform magnetic field exists in the y direction. Electric currents are induced by pulsing a spatially uniform field in the z direction.

Let us define the following parameters:

$A \equiv$ effective loop area (m^2),

$B_y \equiv$ constant magnetic flux density in y direction (T),

$B_z \equiv$ time varying magnetic flux density in z direction (T),

$D \equiv$ mechanical damping constant (N-m-s/rad),

$i \equiv$ total electric current flowing around loop (A),

$I \equiv$ mass moment of inertia ($kg-m^2$),

$k \equiv$ rotational spring constant or stiffness coefficient (N-m/rad),

$L \equiv$ effective loop inductance (H),

$R \equiv$ effective loop resistance (Ω),

$\Gamma_x \equiv$ torque about x axis due to the Lorentz interaction of the current with the magnetic fields (N-m),

$\zeta \equiv$ mechanical damping ratio (dimensionless),

$\theta \equiv$ angle of rotation (rad),

$\Phi \equiv$ magnetic flux through loop (Wb).

Consider a rectangular loop with outer perimeter dimensions ℓ and w, with rectangular cross-sectional dimensions h and a, perpendicular and parallel to the plane of the loop, respectively, and with uniform resistivity ρ (Ω-m). For this system we used the following formula for the loop resistance and area

$$R = 2\rho\,(\ell+w-2a)/(ah) \tag{2}$$

$$A = (\ell-a)\,(w-a). \tag{3}$$

The loop inductance was calculated using a converted formula from Terman,[8]

$$L = \frac{\mu_0}{\pi}\left[(\ell+w)\ln\left(\frac{2\ell w}{a+h}\right) - (\ell)\ln(\ell+g) - (w)\ln(w+g) + 2g - \frac{\ell+w}{2} + 0.447(a+h)\right],$$

where $g = \sqrt{\ell^2+w^2}$ and $\mu_0 = 4\pi\times10^{-7}$. (4)

As mentioned in Sec. II, the comparable formulas for the effective loop resistance, area, and inductance of a rectangular plate were determined empirically using the SPARK code to match the decay time constant, total current, and net torque. Consider a rectangular plate with outer perimeter dimensions ℓ and w, with thickness h, and with uniform resistivity $\rho(\Omega\text{-m})$. For this system we used the following formulas

$$R = 3.33\,\rho(\ell^2+w^2)/(h\ell w) \tag{5}$$

$$A = 0.483\,\ell w \tag{6}$$

$$L = 4.65\times10^{-7}(\ell+w)\ . \tag{7}$$

We can write the applicable mechanical and electrical differential equations for the rigid body rotation of either the loop or the effective loop as

$$I \frac{d^2\theta}{dt^2} + D \frac{d\theta}{dt} + k\,\theta = \Gamma_x \tag{8}$$

$$L \frac{di}{dt} + R\,i = - \frac{d\Phi}{dt} . \tag{9}$$

The mechanical damping constant D is usually seen expressed in terms of the damping ratio ζ as

$$D = 2\zeta \sqrt{kI} . \tag{10}$$

The damping ratio ζ is often multiplied by 100 and referred to as *percent of critical damping*.

The flux passing in a positive direction through the rectangular area A at angle of rotation θ is given by

$$\Phi = AB_z \cos\theta - AB_y \sin\theta \tag{11}$$

and the time derivative of Φ is thus

$$\frac{d\Phi}{dt} = A\dot{B}_z\cos\theta - AB_z\dot{\theta}\sin\theta - A\dot{B}_y\sin\theta - AB_y\dot{\theta}\cos\theta . \tag{12}$$

Similarly, the net torque on a rectangular loop due to the Lorentz forces is given by

$$\Gamma_x = (-B_z\sin\theta - B_y\cos\theta)\,iA . \tag{13}$$

Reference 4 pointed out that we can define a coefficient of $\dot{\theta}$ comparable to the mechanical damping constant which we refer to as the magnetic damping constant, D_{mag}, where

$$D_{mag} = A^2 B_y^2 / R \ . \tag{14}$$

We can similarly define a magnetic damping ratio, ζ_{mag}, as

$$\zeta_{mag} = \frac{1}{2} D_{mag} / \sqrt{kI} \ . \tag{15}$$

If we consider a system where $\theta < 0.15$, $\dot{B}_y = 0$, $B_y >> B_z$, and $\zeta_{mag} >> \zeta$, then we can approximate Eqs. (8) and (9) with

$$I\ddot{\theta} + k\theta + AB_y i = 0 \tag{16}$$

$$-AB_y\dot{\theta} + L\frac{di}{dt} + Ri = -A\dot{B}_z \ . \tag{17}$$

Reference 4 reported that analytical solutions could be obtained for i and θ in Eqs. (16) and (17) by using Laplace Transforms for the case where B_z was a linear ramp, i.e., $\dot{B}_z$= a constant. The dominant term in the coupled oscillations of both i and θ is

$$\omega^2 = k/I + A^2 B_y^2 /(IL) \ . \tag{18}$$

In Eq. (18), since k is the mechanical stiffness coefficient, $A^2 B_y^2/L$ is analogous to a magnetic stiffness coefficient.

In this report we will only consider a vertical field driver exponentially decaying from an initial value, B_{zo}, as

$$B_z = B_{zo}e^{-t/\tau_p} \tag{19}$$

where τ_p is referred to as the driver time constant. The time derivative of B_z is thus

$$\dot{B}_z = - (B_{zo}/\tau_p)\, e^{-t/\tau p} \quad . \tag{20}$$

We can again use the Laplace Transform technique to solve analytically Eqs. (16) and (17) for i and θ with Eq. (20) as the driver. The details are omitted here and only the final results given. Let:

$$\tau = L/R \; ; \quad \omega_\beta^2 = A^2B_y^2/(IL) \; ; \quad \omega_k^2 = k/I \; ; \quad d = -1/\tau_p \; ;$$

$$p = 1/\tau \; ; \quad q = (\omega_\beta^2 + \omega_k^2) \; ; \quad r = \omega_k^2/\tau \; ;$$

$$\alpha = (3q-p^2)/3 \; ; \quad \beta = (2p^3 - 9pq+27r)/27 \; ;$$

$$P = \left[\frac{-\beta}{2} + \sqrt{\left(\frac{\beta^2}{4} + \frac{\alpha^3}{27}\right)}\right]^{1/3} \; ; \quad Q = \left[\frac{-\beta}{2} - \sqrt{\left(\frac{\beta^2}{4} + \frac{\alpha^3}{27}\right)}\right]^{1/3} \; ;$$

$$a = P+Q; \quad b = -\left(\frac{P+Q}{2}\right) + \left(\frac{P-Q}{2}\right)\sqrt{-3}; \quad c = -\left(\frac{P+Q}{2}\right) - \left(\frac{P-Q}{2}\right)\sqrt{-3} \; .$$

In most cases of interest, a will be a real number with b and c complex conjugates. In all cases, the real parts of a, b, and c are negative.

Now let:

$$f = A\, B_{zo}\, d/[L(a-b)(b-c)(c-a)] \quad :$$

$$f_1 = \frac{(b-c)}{(d-a)}\,(a^2+\omega_k^2)f \quad ; \quad f_2 = \frac{(c-a)}{(d-b)}\,(b^2+\omega_k^2)f \quad ; \quad f_3 = \frac{(a-b)}{(d-c)}\,(c^2+\omega_k^2)f \quad ;$$

$$g = -A^2 B_y\, B_{zo}\, d/[IL(a-b)(b-c)(c-a)] \quad ;$$

$$g_1 = \frac{(b-c)}{(d-a)}\, g \quad ; \quad g_2 = \frac{(c-a)}{(d-b)}\, g \quad ; \quad g_3 = \frac{(a-b)}{(d-c)}\, g \quad .$$

We can then write the solutions to Eqs. (16) and (17) in the form

$$i(t) = f_1\,(e^{dt}-e^{at}) + f_2(e^{dt}-e^{bt}) + f_3(e^{dt}-e^{ct}) \tag{21}$$

$$\theta(t) = g_1(e^{dt}-e^{at}) + g_2(e^{dt}-e^{bt}) + g_3(e^{dt}-e^{ct}) \; . \tag{22}$$

IV. EXPERIMENTAL SETUP

A. FELIX facility

FELIX is an experimental test facility constructed at ANL for the study of electromagnetic effects expected to be encountered in fusion reactor systems. A detailed description of FELIX was presented by Praeg *et al.*[9] Figure 2 illustrates the two electromagnet subsystems of FELIX and the available experimental volume.

The two electromagnets are referred to as the solenoid and dipole. The solenoid subsystem consists of four solenoidal coils which are physically separated to provide access to the test volume. The solenoid coils produce a highly uniform, horizontal magnetic field over the test volume. The dipole subsystem consists of two pairs of saddle coils located on the top and the bottom of the solenoidal coils. The dipole coils produce a highly uniform, vertical magnetic field over the test volume. Since the test pieces we employed in these experiments occupied only the central portion of the available test volume, we expected the field variation to be less than 4% within the test piece envelope for either the dipole or solenoid field.

The solenoid and dipole are powered by separate power supplies. The dipole was driven to a flattop value which lasted for about eight seconds to allow any initial eddy currents to decay completely. The dipole coils were then switched using a thyristor circuit from the power supply to a resistor array. The current in the dipole coils then decayed exponentially as determined by the dipole resistor value and produced the eddy currents of interest in this investigation.

During the coupled tests, the solenoid field was employed in addition to the dipole field. The same time sequence was used for the dipole. After about 5.5 secs of the dipole flattop, the solenoid current was turned on and increased so that the solenoid field was just at full value when the dipole switching occurred. The solenoid field was kept at its full value for a two-second flattop.

B. Test fixture

An isometric view of the test fixture used in this series of experiments is shown in Fig. 3. The basic structure consists of a nonconducting square test piece holder between two nonconducting tubes which are each mounted in a roller bearing system. G-10 was used for the nonconducting material of the frame and the tube. A test piece was clamped in the holder by 28 nylon bolts. The bearing system consisted of a Teflon cage containing brass rollers that rolled directly between the tube and an outer nylon race. The fixture dimensions are indicated on Fig. 3.

At each end of the fixture an aluminum collar was bolted around the tube to attach a pair of phosphor bronze leaf springs. The springs are also shown on Fig. 3. Each spring passed through a pair of nonrotating cylindrical guides which could be set various distances from the axis to allow a range of spring constants. The two guide positions used in the experiment are illustrated in Fig. 4. The diameter of each guide was 19.05 mm (0.750 in) and an average gap was provided between the guides that was 0.33 mm (0.013 in) larger than the spring thickness 3.175 mm (0.125 in). Each pair of guides was mounted in a U-bracket which was bolted to a stainless steel track. Shims were used to make the gap as uniform as possible.

The purpose of the gap between the guides and the spring was to allow the spring to move freely longitudinally and behave as closely as possible to a simple harmonic oscillator characterized by one fundamental frequency. Each guide track was bolted to a stainless steel pillar and through stiffener columns to the floor. The entire support system for the test piece was

mechanically isolated from the coil systems. Emphasis was placed on ensuring that the test piece holder, axle tubes, and all connecting and supporting hardware were extremely rigid compared to the leaf springs. This was desired to both ensure a single frequency system and to minimize the mechanical damping ratio to at most a few percent of critical damping.

C. Test pieces

Two different types of test pieces were used in this experiment, a square loop and a square plate. The outside dimensions of both the loops and plates were 0.5 m x 0.5 m (19.685 in x 19.685 in). The minor cross section of each loop was 25.4 mm x 25.4 mm (1.0 in x 1.0 in). The thickness of each plate was 6.35 mm (0.25 in).

Each test piece was designed to accommodate a Rogowski coil for measuring the total current flowing around the piece. Each plate had a 50.8 mm (2.0 in) hole at the center so the coil would not interfere with test piece movement. The relatively small hole at the center was expected to have a negligible effect on the eddy current distribution.

Two loops and two plates were tested: a copper loop, $\rho = 1.726 \times 10^{-8}$ Ω-m; a bronze loop, $\rho = 6.63 \times 10^{-8}$ Ω-m; a copper plate, $\rho = 1.726 \times 10^{-8}$ Ω-m; and a stainless steel plate, $\rho = 7.2 \times 10^{-7}$ Ω-m.

D. Instrumentation

1. Minicomputer system

A Data General minicomputer system was used for data acquisition. Data were initially recorded on a hard disk, later transferred to another storage disk, and also backed up on floppy disks. Up to ten tracks were recorded per shot with each track containing 2048 data values. The data collected during these experiments were transferred from the minicomputer to an IBM mainframe at ANL and then transferred via the BITNET computer network to an IBM mainframe at Princeton University.

During the fully coupled shots and the dipole-only shots, the data rate was 100 Hz for approximately the first 8 secs until just before the dipole pulse. After that time during the coupled shots, the data rate was 500 Hz; but during the dipole-only shots, the data rate generally was 5000 Hz, except for a few initial shots at 500 Hz. For the mechanical dynamic tests, the data rate was 500 Hz throughout.

2. Rotational transducer

A Schaevitz Engineering rotational linear differential transformer (LVDT) was mounted on a small radius central shaft which mechanically coupled to the central axis at one end of the test fixture. Comparison of the output signal with survey measurements showed the signal to be very linear over the range of the experiment and accurate to within at least two mrads and probably much better in most cases.

3. Rogowski coil - test piece

The test piece Rogowski coil had a major radius of 192 mm, minor radius of 3.7 mm, and was wound with 4087 turns of #30 enameled copper wire. Calibration of this coil with a known bus yielded a ratio of 3.67 kA/V with an integration time constant of 10 msec.

4. Rogowski coil - dipole bus

A smaller Rogowski coil was used to find the current in the dipole coils by measuring the current in a dipole bus bar. This Rogowski coil had a major radius of 55 mm, minor radius of 17 mm, and was wound with 1532 turns of #30 enameled copper wire. Calibration of this coil with a known bus yielded a ratio of 1.10 kA/V with an integration time constant of 10 msec. Only one Rogowski coil could be recorded per shot because only one integrator circuit was available.

5. Other measurements

During each test shot, a multiaxis hall probe was positioned as near as possible to the test piece center to record both the vertical (z) and horizontal (y) magnetic fields. In addition, the voltage signals were recorded from shunts installed on the dipole power supply main bus, the dipole resistor, and the solenoid bus.

V. MECHANICAL TESTS

A. Spin tests

Considerable care was taken to reduce the bearing friction to an acceptable value. The final design was checked with no springs or clamps on the axle so that the fixture could rotate 360 degrees. The entire fixture was first aligned with surveying instruments to within ± 1 mm. The test piece holder was rotated to various angles and checked for balance. No movement was observed with the holder at any angle. The holder with no test piece was then given a moderate push to observe the number of rotations the fixture made before coming to rest. The final design rotated almost three complete rotations, which we felt adequate for our purpose.

B. Static tests

With the springs installed, the guides were set at various positions to calibrate the available range of spring constants. A $1/4$-inch thick aluminum L-channel, 153 inches long, was clamped symmetrically to the test piece holder. At one end of the beam a measured weight was attached pulling downwards and at the other end a rope and pulley arrangement was used to apply an identical force upwards. The static rotation was measured using surveying instruments. At the same time, the survey measurements were used to calibrate the rotational transducer. In addition, during the static tests four strain gauges were installed on one of the springs at the locations expected to be in maximum stress. The stress measurements were used to fix a maximum deflection angle at each spring constant setting.

The static deflection values versus applied moment yielded very linear plots. Measurements were taken at nominal spring constants of 3, 9, 15, and 30 kN-m/rad. The two values selected for the operational tests were 3 and 9 kN-m/rad and are abbreviated in the recorded data as 3 kN and 9 kN. The actual measured spring constants were 2830 and 8700 N-m/rad, respectively. Maximum deflections were limited to 0.105 and 0.045 rad, respectively.

C. Dynamic mechanical tests

The dynamic mechanical tests were performed to measure the natural mechanical frequency of vibration, ω_k, the mechanical damping ratio, ζ, and the moment of inertia, I. The tests were performed after rotating the test fixture to an initial rotation, θ_o, using a similar setup as the static tests. A simple system which is initially displaced in this manner at time zero would be expected to decay as

$$\theta = \frac{\theta_o}{\sqrt{(1-\zeta^2)}} e^{-\zeta\omega_k t} \cos(\omega_D t - \phi), \tag{23}$$

where $\omega_D = \omega_k\sqrt{(1-\zeta^2)}$ and $\phi = \sin^{-1}(\zeta)$.

The observed data were matched to Eq. (23) using ZXSSO, a least squares residual sum FORTRAN subroutine for nonlinear equations found in the IMSL (International Mathematical and Statistical Library) package. Figure 5 gives two examples of the calculated curves compared with the observed data. Note that the first oscillation or two were not fitted in order to avoid the influence of second order vibrations. The nominal 3 kN position proved to be

an excellent match to this equation for all the test pieces. The damping ratios were calculated to be about 1%. Stiffer spring positions provided progressively increasing contributions from vibratory modes beside the fundamental. The nominal 9 kN seemed to be the limit of reasonable fit. In the nominal 9 kN position, when the initial 500 points of a shot were compared with later 500 point sets, the damping ratio was observed to increase by a factor of 2 or 3 from the beginning to the end of a shot. The values obtained by fitting the first 500 points were used in the subsequent analysis. A table of the results appears below.

k	3 kN (2830 N-m/rad)			9 kN (8700 N-m/rad)		
	ω_k	ζ	I	ω_k	ζ	I
Copper Loop	41.2	0.010	1.67	70.7	0.015	1.74
Bronze Loop	41.8	0.013	1.62	72.2	0.014	1.67
Copper Plate	42.4	0.013	1.57	72.9	0.019	1.64
Stainless Plate	42.6	0.012	1.56	73.4	0.011	1.61

During the preoperational phase of the experiments, several initial positions, θ_0, were tested at each spring constant to assure ourselves that the measured mechanical parameters did not change over the range of deflections investigated. The table shows that the variation of the mechanical parameters among the test pieces was small. Note, however, that the moment of inertia, I, consistently increased from the 3 kN to the 9 kN spring position.

VI. DIPOLE-ONLY TESTS

Each test piece was tested with the test fixture in its neutral position by pulsing the dipole field only. We measured induced currents, but observed no rotation of the test piece. The dipole field was pulsed at nominal initial values of 25 mT and 50 mT with nominal decay times of 10, 20, 40, and 100 ms.

Figure 6 shows some representative current measurements obtained from the dipole resistor shunt for the nominal 50 mT initial field decaying at 10, 20, 40, and 100 ms. The time scale is compressed for approximately the first 0.165 seconds on each graph during which the sampling rate was 100 Hz. The sampling rate for the remainder of each shot was 5000 Hz. From about 0.18 to 0.20 seconds a high frequency pulse is observed that results from the thyristor switching transition. The switching transition is terminated by a sharp spike due to the discharge of the high voltage power supply capacitor. The remainder of the signal shows the dipole current decaying in combination with some predominately 60 Hz power supply ripple.

During the tests with the copper loop for the 9 kN spring position, the high voltage capacitor was set at 9 kV. This setting produced a very large spike in the test piece Rogowski signal. After this first series of tests, the high voltage was set at 2 kV for the 25 mT field and at 4 kV for the 50 mT field. These settings diminished the magnitude of the spikes considerably.

It will be observed in the subsequent graphs for both coupled and uncoupled shots that the switching transition and the accompanying discharge spike induces currents in the test piece. In the coupled cases, these

currents also produce mechanical motion. For the 10 ms decay time constant tests, the magnitude of the current induced by the switching transition is small compared to the primary signal. As the decay time constant becomes longer, the switching currents become more comparable to the primary signal and hence the induced currents and motion from the switching become more comparable to the primary signal. Qualitatively, the 10 ms cases have the least second order effects while the 100 ms cases have the most second order effects. Similarly, the primary to secondary signal ratio is higher for the nominal 50 mT case than the nominal 25 mT case.

Figure 7 shows the currents measured by the Rogowski coil around the dipole bus bar for the same 50 mT initial field decaying at 10, 20, 40, and 100 ms and for the same sampling rates as in Fig. 6. The currents actually flowing in the dipole coils due to the switching transiton and discharge spike are seen in Fig. 7 to be nearly equal for each of the decay time constants.

The IMSL subroutine ZXSSO, previously mentioned in Sec. V.C., was used to fit exponentially decaying curves to the dipole bus Rogowski coil data for both the 25 mT and 50 mT cases. Only one parameter, the decay time constant, was fitted for each curve. Figure 8 shows the results for the 50 mT data shown in Fig. 7. Note that the data selected for fitting starts after the spike when the current is first equal to or greater than the current peak before the spike. The following table summarizes the extracted time constants:

	Nominal τ_p			
Nominal B_{zo}	10 ms	20 ms	40 ms	100 ms
25 mT	11.6 ms	21.1 ms	37.9 ms	101.5 ms
50 mT	11.7 ms	21.6 ms	39.0 ms	106.3 ms

The variation in the time constants is, as expected, greater for the longer time constants. The 50 mT results were selected for use in all the subsequent analysis because they seemed less perturbed by second-order effects.

When the test pieces are subjected only to the dipole field pulse, i.e., By = 0, Eq. (21) reduces to the form:

$$i(t) = \frac{AB_{zo}}{R(\tau-\tau_p)} \left[\exp\left(\frac{-t}{\tau_p}\right) - \exp\left(\frac{-t}{\tau}\right)\right] \quad , \text{ if } (\tau_p \neq \tau)$$

$$= \frac{AB_{zo}\, t}{R\, \tau\, \tau_p} \exp\left(\frac{-t}{\tau_p}\right) \quad , \qquad \text{if } (\tau_p = \tau). \tag{24}$$

The integrated test piece Rogowski coil signal for the dipole-only tests for the copper loop and copper plate were fitted to Eq. (24) with B_{zo} as the one unknown value. This signal always began a shot at zero value but finished with an offset value. Time zero was chosen at the discharge spike if the spike did not dip below the offset otherwise at the point when the current first reached the offset value after the spike. The extracted B_{zo} values for the nominal B_{zo} values for the copper loop and copper plate are given in the following table. The copper plate results are in parentheses.

Nominal B_{z0}	Nominal τ_p 10 ms	20 ms	40 ms	100 ms
25 mT	33.2 mT	32.5 mT	32.2 mT	28.6 mT
50 mT	56.6 mT	56.0 mT	55.0 mT	49.9 mT
(25 mT)	(33.5 mT)	(33.1 mT)	(32.5 mT)	(31.1 mT)
(50 mT)	(56.0 mT)	(55.3 mT)	(53.7 mT)	(49.6 mT)

The values of B_{z0} were also determined from the dipole bus current and the vertical Hall probe measurements. These values were calibrated to the central field and were not necessarily identical to the average field values across the area of the test piece. Preliminary FELIX design computations showed the expected variation across a test piece to be less than 0.5% of the central field. All the measurements agreed to within this limit.

The Hall probes showed fields from 33-35 mT and 54-56 mT. The fields calculated from the dipole bus current measured by the small Rogowski coil were 33.3 and 53.9 mT. These measurements were subject to instrument and alignment errors, but the mutual agreement between the measurements and fitted values was very good. In all subsequent calculations the values of 33 and 56 mT were used for the nominal 25 and 50 mT cases, respectively. Figure 9 shows the selected data points compared to the predicted curves for the nominal 25 mT copper loop tests.

Additional curve fitting was done for the bronze loop, copper plate, and stainless steel plate. In these cases the resistance R was extracted as the unknown value. For the copper plate the predicted R was 18.1 μΩ. The extracted values were:

Nominal B_{zo}	Nominal τ_p 10 ms	20 ms	40 ms	100 ms
25 mT	17.9 μΩ	18.5 μΩ	18.8 μΩ	19.1 μΩ
50 mT	18.4 μΩ	18.6 μΩ	19.0 μΩ	20.1 μΩ

For the bronze loop and stainless steel plate, the test piece Rogowski signals became very small compared to noise signals, particularly as the time constant became longer. In fact only the nominal 10 ms case was usable for the stainless steel plate. For the bronze loop the predicted R was 195 μΩ. The extracted values were:

Nominal B_{zo}	Nominal τ_p 10 ms	20 ms	40 ms	100 ms
25 mT	264 μΩ	287 μΩ	*	*
50 mT	249 μΩ	269 μΩ	320 μΩ	983 μΩ

For the stainless steel plate, the predicted R was 755 μΩ. The extracted values were 2410 and 2100 μΩ for the nominal 25 mT and 50 mT cases, respectively.

The extracted values for the copper plate were so close to the predicted values that the original formula values for the test pieces were used in the subsequent analysis. The discrepancies related to the bronze loop and stainless steel plate represented small signal values and were attributed to instrument error. Figure 10 shows the nominal 10 ms, 25 mT case for each test piece, plotted to the same scale, comparing the observed data points to the predicted curve.

VII. COUPLED TESTS

In a similar manner to the dipole field calibration described in the previous section, the solenoid field was determined for the coupled tests. The nominal solenoidal field values used in the tests were 200, 400, and 800 mT. Measurements for the coil current of the solenoid and the Hall probe horizontal component were subject to some instrument error and misalignment. In addition, at the nominal 800 mT field, the coil current exceeded our measurement capability even at the lowest amplifier gain setting available. Preliminary FELIX design computations predicted the variation in the solenoid field across the test piece to be less than 4% of the central value.

The coupled tests for the nominal 10 ms copper loop were chosen to extract the solenoid field values. Again using the IMSL subroutine ZXSSQ, we extracted the single parameter B_y. In the coupled tests, measurements were taken for both rotation angle and test piece current so both Eqs. (21) and (22) were fitted. The extracted B_y values are summarized in the following table:

		Nominal B_y			
k	B_{zo}	200 mT	400 mt	800 mT	(fit)
3 kN	25 mT	220.3 mT	421.9 mT	854.9 mT	(θ)
3 kN	25 mT	215.0 mT	415.9 mT	887.3 mT	(i)
9 kN	50 mT	212.7 mT	421.7 mT	798.4 mT	(θ)
9 kN	50 mT	205.0 mT	419.1 mT	783.9 mT	(i)

In comparison, the B_y values measured by the Hall probe peaked at about 202-214, 405-407, and 808 mT for the nominal 200, 400, and 800 mT cases, respectively. Similarly, the B_y values calculated for the central field from the solenoid current were 198.6 and 396.2 mT for the nominal 200 and 400 mT cases, respectively. The power supply control settings for the nominal field values provided confidence that the final field values should be in the ratios of 1:2:4 among the 200, 400, and 800 mT cases.

The extracted B_y values in the above table show good agreement for the nominal 200 and 400 mT cases. The nominal 800 mT values show a wider variation, but less weight is given to these measurements, particularly at the stiffer spring setting. This subject will be addressed in the next section on second order effects. The values 210, 420, and 840 mT were used for the nominal 200, 400, and 800 mT cases in all subsequent calculations.

The coupled tests were conducted with the nominal dipole field values of 25 and 50 mT combined with the nominal dipole field time constants of 10, 40, and 100 ms. For the copper loop, nominal solenoid field values of 50 and 100 mT were employed in lieu of the nominal 400 and 800 mT values in order to avoid excessive rotation at the nominal 3 kN spring position with the nominal 10 ms time constant.

Some shots were omitted at the longer time constants for both the bronze loop and the stainless steel plate, because of the negligible signals produced. The signal from the test piece Rogowski coil was not usable for any of the coupled shots with the stainless steel plate.

Oscilloscope photographs were taken of the angle and/or current traces for all the shots. The traces were examined to ensure that the shot was not missed and that the data were repeatable. The neutral position reading of the rotational transducer was recorded for each shot to guard against systematic drift. Similarly, test fixture alignment marks were checked throughout the tests and each test piece was checked with a level after each spring adjustment.

Figures 11-16 present some representative data for the copper loop and copper plate for the coupled tests with a decay time of 11.7 ms. The observed data are indicated by the asterisks. The complete predicted solutions including mechanical damping obtained by solving Eqs. (8) and (9) numerically are indicated by the dashed lines. The simplified analytic predicted solutions from Eqs. (21) and (22) are shown by the solid lines. The agreement of both the angle and current predictions with the measured values is excellent for the nominal 200 and 400 mT solenoid field cases. The 800 mT solenoid field cases produce the most disagreement, but the basic characteristics of the predicted curves are preserved.

For comparison, Fig. 17 shows two of the copper plate cases with their corresponding uncoupled solutions indicated by dashed lines. The significant differences obtained by omitting the coupled terms are readily apparent.

The same general observations made for the representative curves here also apply to the other decay times and the other test pieces. The 3 kN spring data are generally in slightly better agreement than the 9 kN spring data. The observed curves generally damp out more quickly than predicted,

except in the case of the copper loop at the 9 kN spring position. Recall that these tests were conducted with a high voltage setting of 9 kV. The response due to the high voltage spike in many of these shots is greater than or comparable to the predicted response. This is clearly evident in the longer time constant shots for the copper loop at the 9 kN spring. The reduced voltage setting for the remaining tests eliminated this problem.

VIII. SECOND-ORDER EFFECTS

All the shots were repeated for the mechanical, dipole-only, and coupled tests. The mechanical tests depended on a human triggering mechanism, but still gave reproducible extracted parameters. The dipole-only and coupled tests produced essentially duplicate data in repeated shots.

For a given test piece, high frequency perturbations were noted at the stiffer spring position and/or at higher solenoidal fields. The observed perturbations were repeatable, however, as illustrated in Fig. 18. The figures show the copper loop coupled test (nominal 9 kN, 10 ms, 50 mT, 800 mT), DF9K007, shown before in Fig. 13, and its repeated shot, DF9K008, at the same scale. This case represents the worst disagreement which was observed.

Examination of Fig. 18 will show that except for a small difference in the high voltage spike magnitude no difference can be found in the electrical response, but some small, very high frequency mechanical differences exist. Note that the principal residual ripple is found in both the mechanical and electrical signals. This shows that the test piece is moving and we are not just seeing the spring or rotational transducer rattling about as the test

piece remains stationary. The filtering action of the test piece Rogowski coil system does, however, eliminate the very high frequency electrical responses.

We have already mentioned some of the expected sources of perturbation and our efforts to minimize any second order effects. Recall that the spring system has higher order modes than the fundamental, the plates had holes in the center, the dipole and solenoid fields were not perfectly uniform, and the current in the dipole coil system was not a constant value followed by a perfect exponential decay. Although effort was spent to ensure that testing was within the linear range of the springs, the gaps between the springs and guides introduced nonlinear effects as did frictional losses. We observed, however, that over the parameter range of our experiments, most of these effects were truly second order or third or fourth.

No experiments were designed to investigate these second order effects and no attempt was made to include them in the analysis. An interesting, qualitative observation can be made, however, from the observed residual ripple frequencies at the high solenoid field values. Recall in Eq. (18) that $A^2B_y^2/L$ was analogous to a magnetic stiffness coefficient. It follows that increasing the solenoid field, increases the coupled system stiffness, which tends to enhance the excitation of higher order modes. This feature was generally observed throughout the coupled tests.

Reviewing Fig. 17 one estimates that the residual frequency is about 35 Hz for the copper loop at the nominal 9 kN position, B_y = 800 mT. At the same nominal parameters, examination of Fig. 16 will show the copper plate has

about the same residual frequency. Similarly, at the nominal 3 kN position, B_y = 800 mT, the copper plate residual is about 80 Hz, as can be found from Fig. 16. The same trend continued in a preoperational test with a copper loop at a measured 20 kN position, nominal B_y = 800 mT, with the mechanical response measured only. The observed residual was about 19 Hz.

At first it seemed unlikely that stiffer spring positions produced lower second-order modes, but examination of Figs. 3 and 4 revealed a possible source. Note that when the guides are moved inward, the end of the spring is still in the system cantilevered over the guide. This cantilever would be expected to have a lower frequency fundamental as the guides were moved to the stiffer positions. The cantilever is not rigidly clamped by the guides, however, and so the system will give a more complicated response than a simple cantilever, but rough calculations show the expected frequencies to be in the observed range. Recall that in the mechanical tests the moment of inertia increased at the stiffer spring settings. Note also that the magnitude of the test piece ripple movement is very small.

IX. CONCLUSION

A series of experiments was successfully conducted to investigate the quantitative responses of magnetomechanically coupled square loops and plates. The test pieces were rigidly mounted in a fixture suspended by a rotational spring system primarily characterized by a single fundamental mode of vibration. Electrical currents were induced by an exponentially decaying vertical magnetic field. Net torques were created by a constant horizontal field. Accurate measurements were made of the angle of rotation and the total

current flowing around the test piece versus time. Initial mechanical and electrical tests determined the basic system parameters and provided an additional calibration on the power supply related instrumentation and Hall probe measurements.

The coupled tests agreed very well with the predicted responses for both the loops and plates. The expected magnetic stiffness and magnetic damping effects were both observed. The simplified solution obtained by using small angle approximations proved to be very accurate over the parameter space of the experiments.

ACKNOWLEDGMENT

This work was supported by U.S. Department of Energy Contract Nos. DE-AC02-76-CH0-3073 and W-31-109-Eng-38.

REFERENCES

[1]D. W. Weissenburger, J. M. Bialek, G. J. Cargulia, M. Ulrickson, M. J. Knott, L. R. Turner, and R. B. Wehrle, Princeton Plasma Physics Laboratory Report No. PPPL-2159 [Argonne National Laboratory Report No. ANL-FPP-84-3], 1984.

[2]D.W. Weissenburger, Princeton Plasma Physics Laboratory Report No. PPPL-2040, 1983.

[3]NASTRAN is a registered trademark of the National Aeronautics and Space Administration (NASA). MSC/NASTRAN is a version of NASTRAN which has been developed and is maintained by the MacNeal-Schwendler Corporation, 7442 North Figueroa Street, Los Angeles, California 90041.

[4]J. Bialek, D. Weissenburger, M. Ulrickson, and J. Cecchi, in Proceedings of the 10th Symposium on Fusion Engineering, Philadelphia, 1983 (IEEE, New York, 1983), pp. 51-55.

[5]L. Sevier, M. F. Ho, J. Citrolo, J. Bialek, and D. Weissenburger, in Proceedings of the 10th Symposium on Fusion Engineering, Philadelphia, 1983 (IEEE, New York, 1983), pp. 1072-76.

[6]L. R. Turner and J. W. Cuthbertson, Argonne National Laboratory Report No. ANL/FPP/TM-176, 1983.

[7]L. R. Turner and R. J. Lari, IEEE Trans. Magn., MAG-19, 2577 (1983).

[8]F. E. Terman, Radio Engineers Handbook, 1st ed. (McGraw-Hill, New York, 1943), p. 53.

[9]W. F. Praeg, L. R. Turner, J. Biggs, J. Bywater, R. Fuja, M. Knott, R. J. Lari, D. G. McGhee, and R. B. Wehrle, in Proceedings of the 9th Symposium on Engineering Problems of Fusion Research, Chicago, 1981, edited by Chan K. Choi (IEEE, New York, 1981), pp. 1763-66.

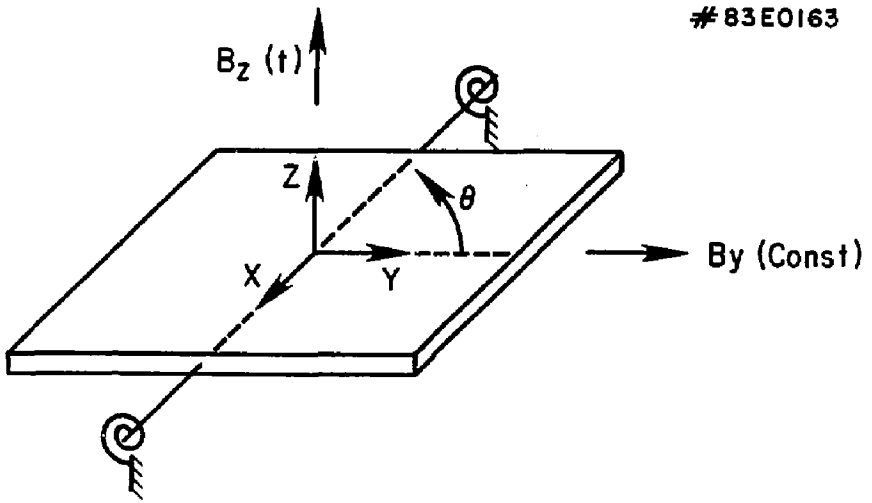

FIG. 1. Basic rectangular plate model.

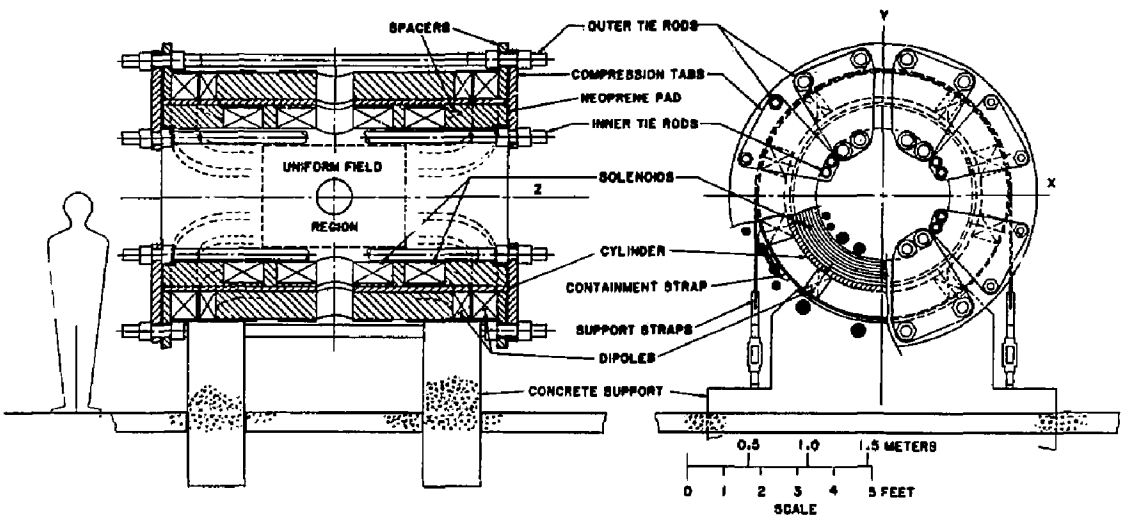

FIG. 2. FELIX facility.

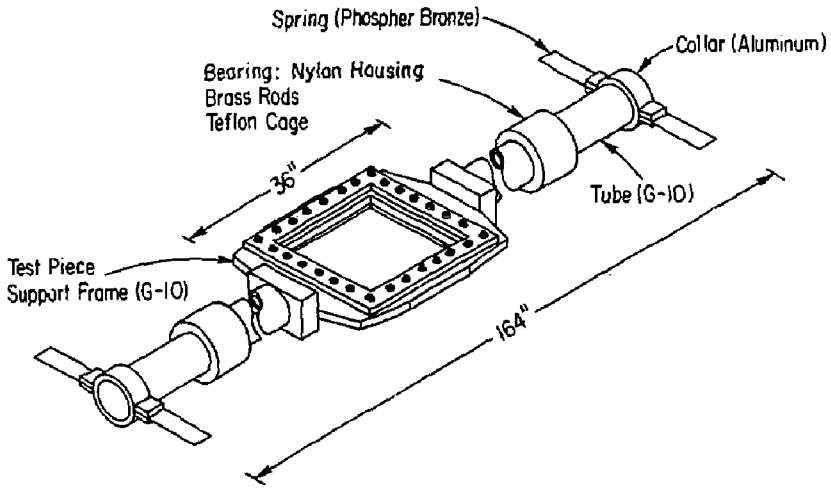

FIG. 3. Test fixture with loop.

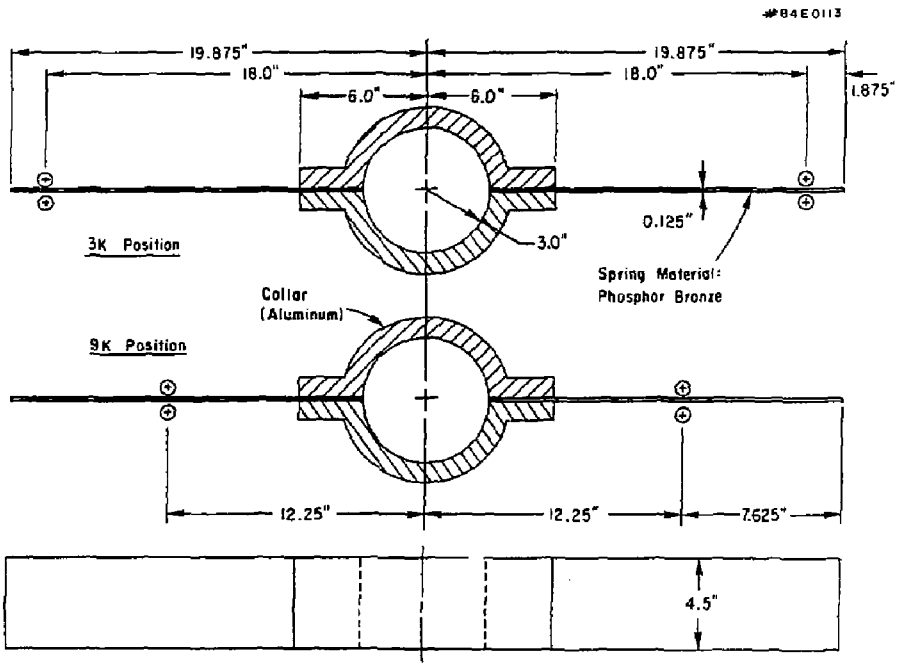

FIG. 4. Guide positions used in tests.

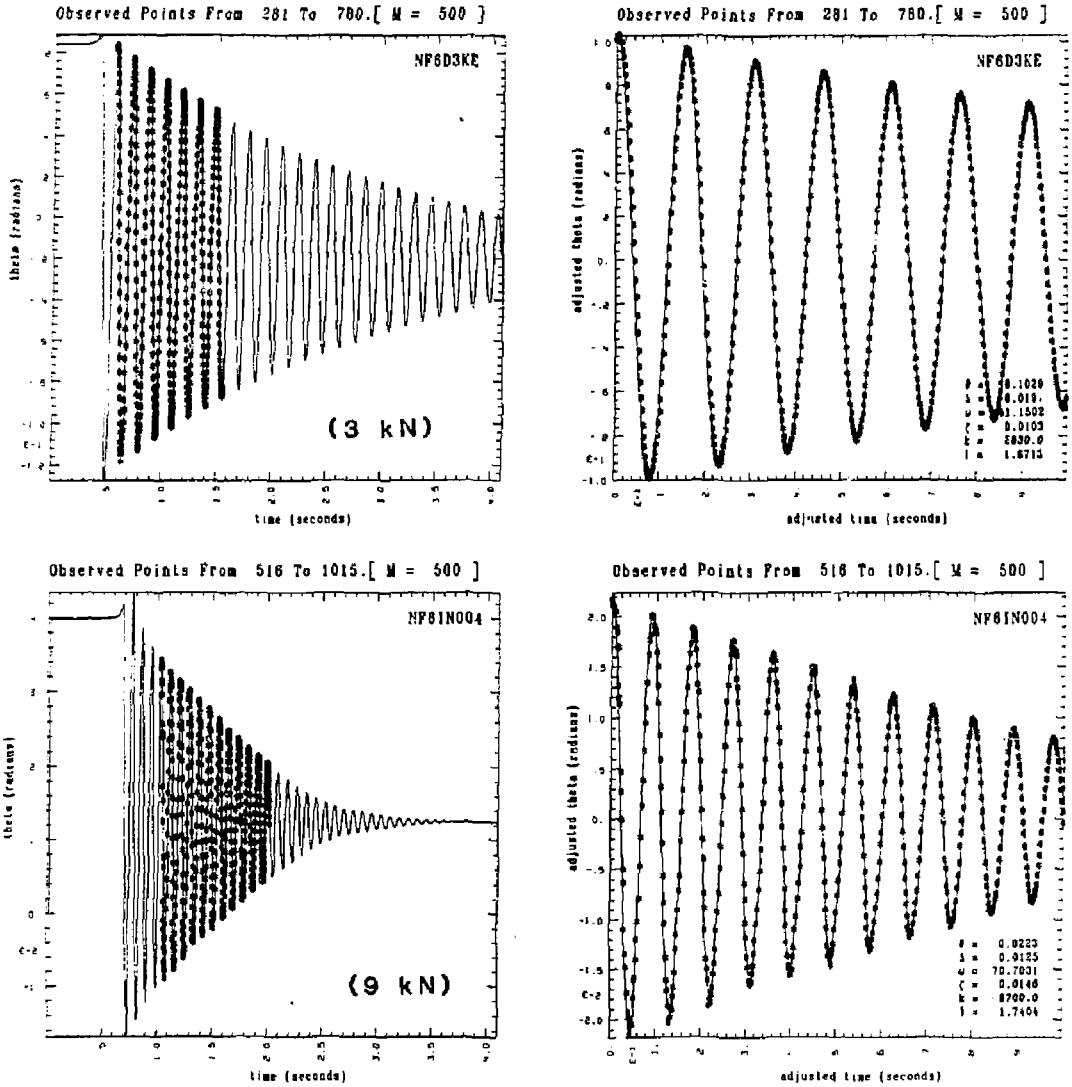

FIG. 5.

Mechanical Damping Tests: Copper Loop.

Nominal Spring Constants Indicated in Parentheses.

Asterisks = selected observation points.
Solid line (left) = observed data.
Solid line (right) = fitted curve.

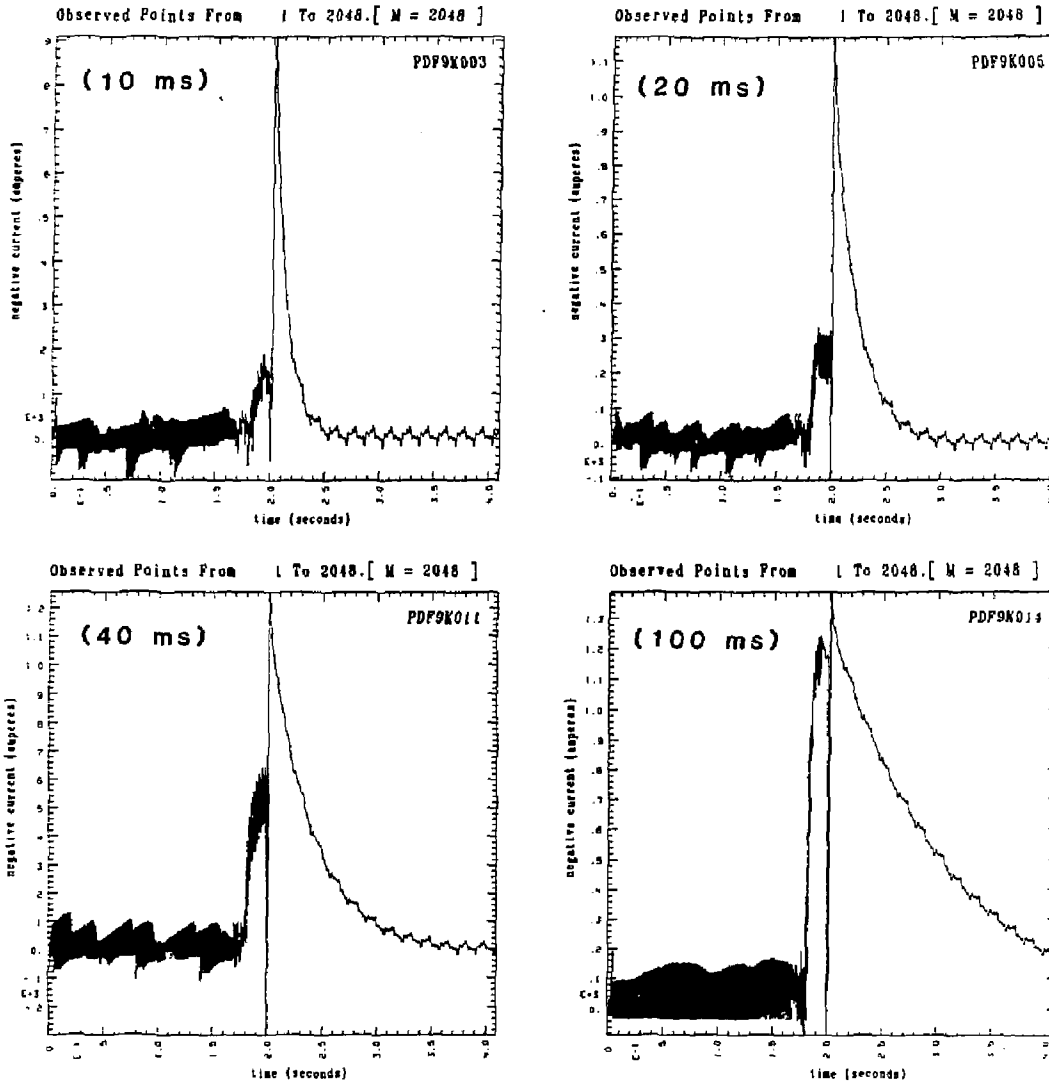

FIG. 6.

56 mT (nominal 50 mT) Dipole-Field-Only Tests:
Dipole resistor shunt measurements.
Nominal decay times indicated in parentheses.

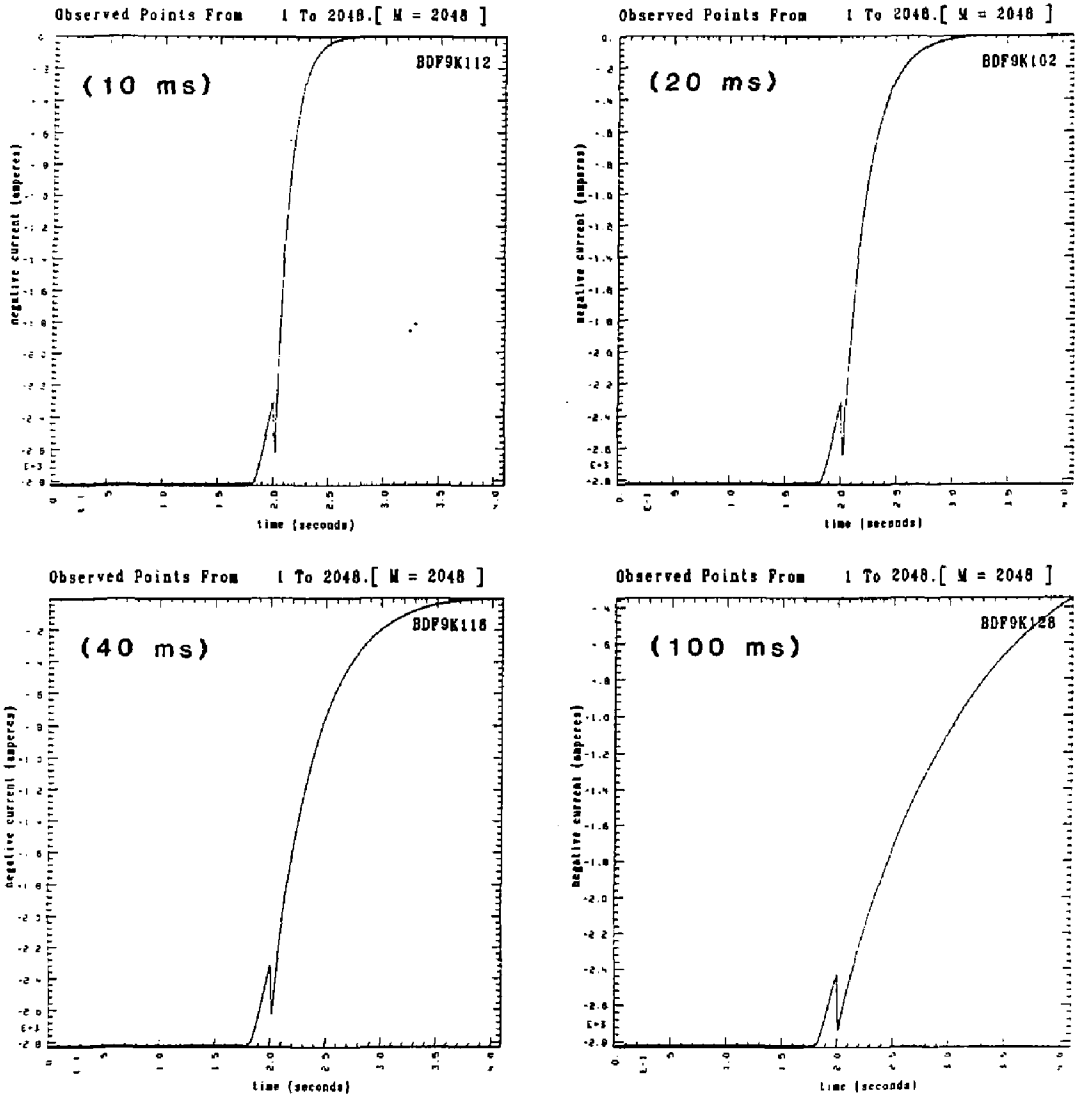

FIG. 7.

56 mT (Nominal 50 mT) Dipole-Field-Only Tests:
Dipole bus Rogowski measurements.
Nominal decay times indicated in parentheses.

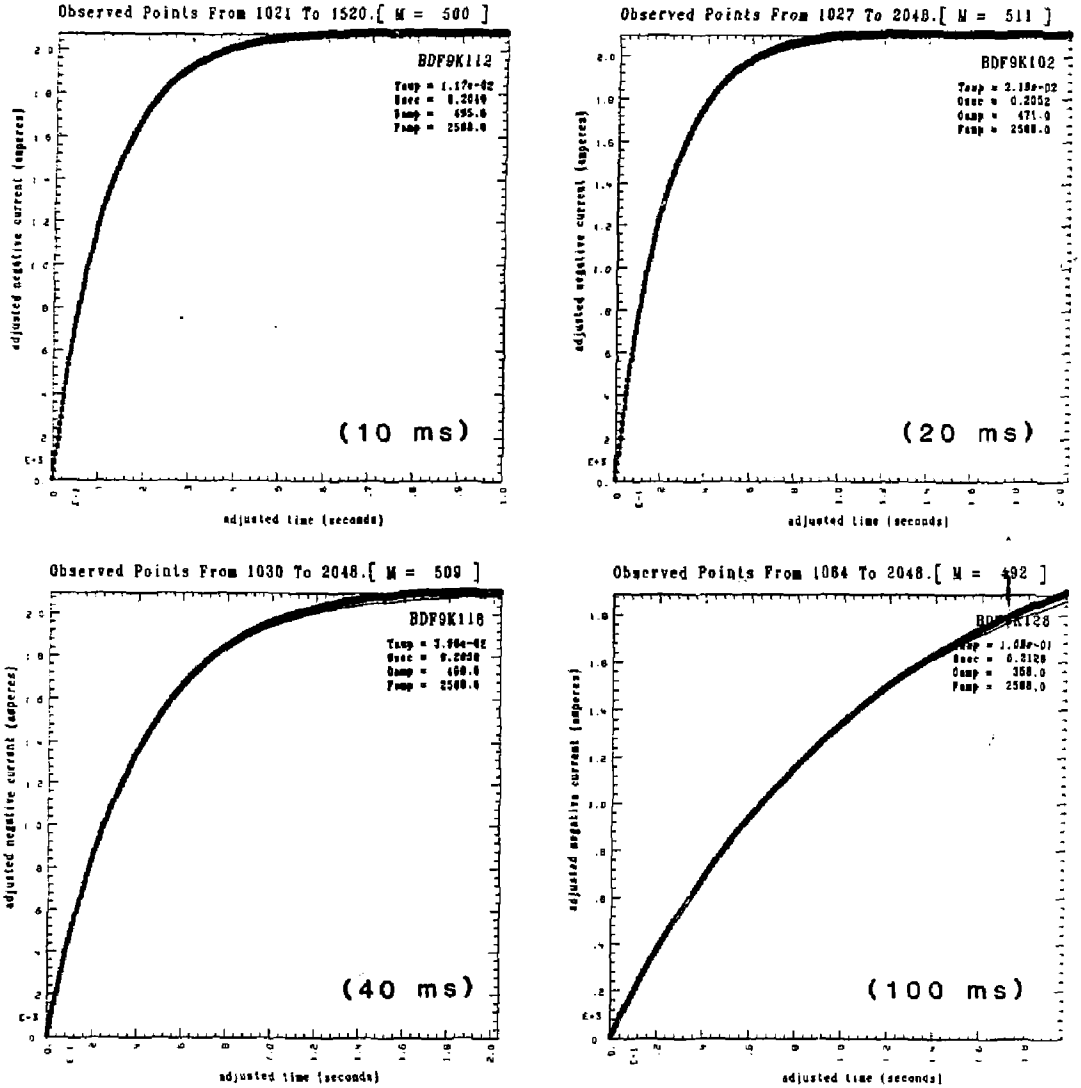

FIG. 8.

56 mT (Nominal 50 mT) Dipole-Field-Only Tests:
Dipole bus Rogowski measurements and predicted curves.
Nominal decay times indicated in parentheses.

Asterisks = observed data.
Solid line = predicted curve.

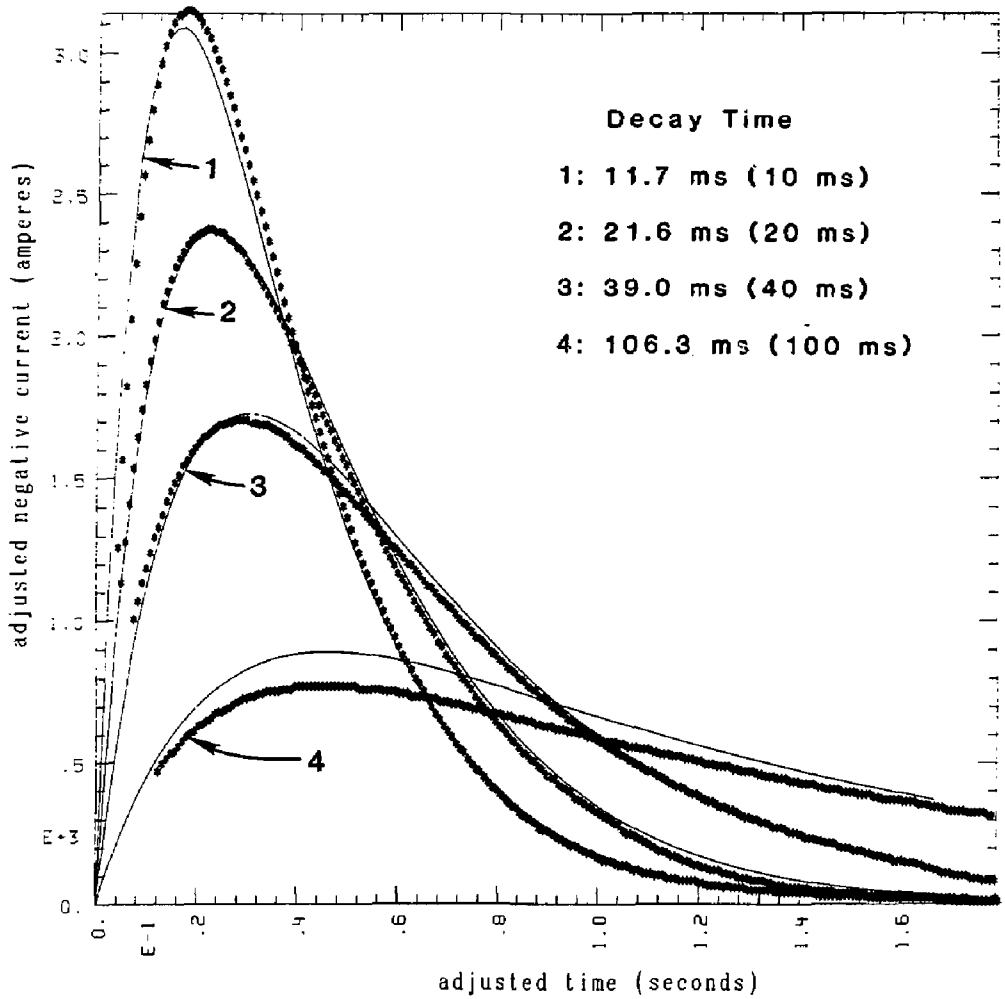

FIG. 9.

33 mT (nominal 25 mT) Dipole-Field-Only Tests: Copper Loop.

Test piece Rogowski measurements and predicted curves.
Nominal decay times indicated in parentheses.

Asterisks = observed data.
Solid line = predicted curve.

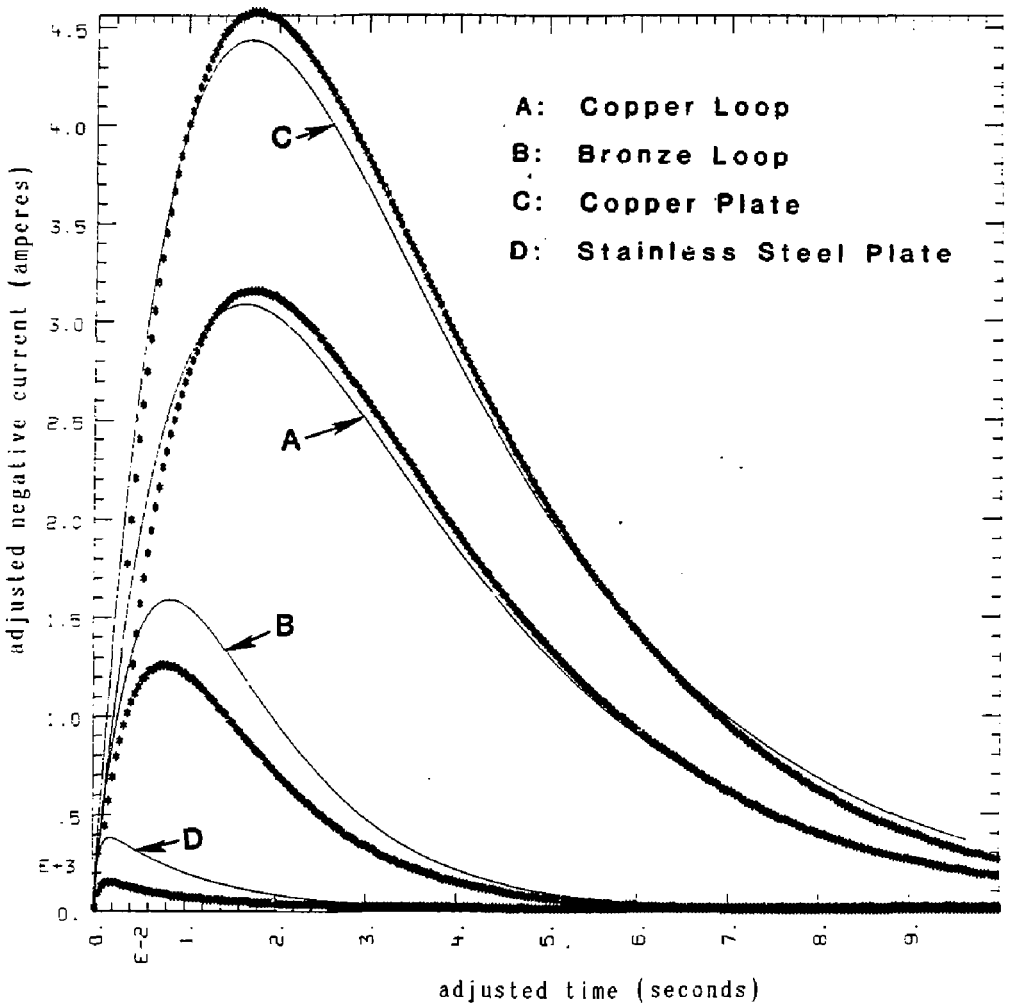

FIG. 10.

33 mT (nominal 25 mT) Dipole-Field-Only Tests and Predicted Curves.
11.7 ms (nominal 10 ms) decay time.

Asterisks = observed data.
Solid line = predicted curve.

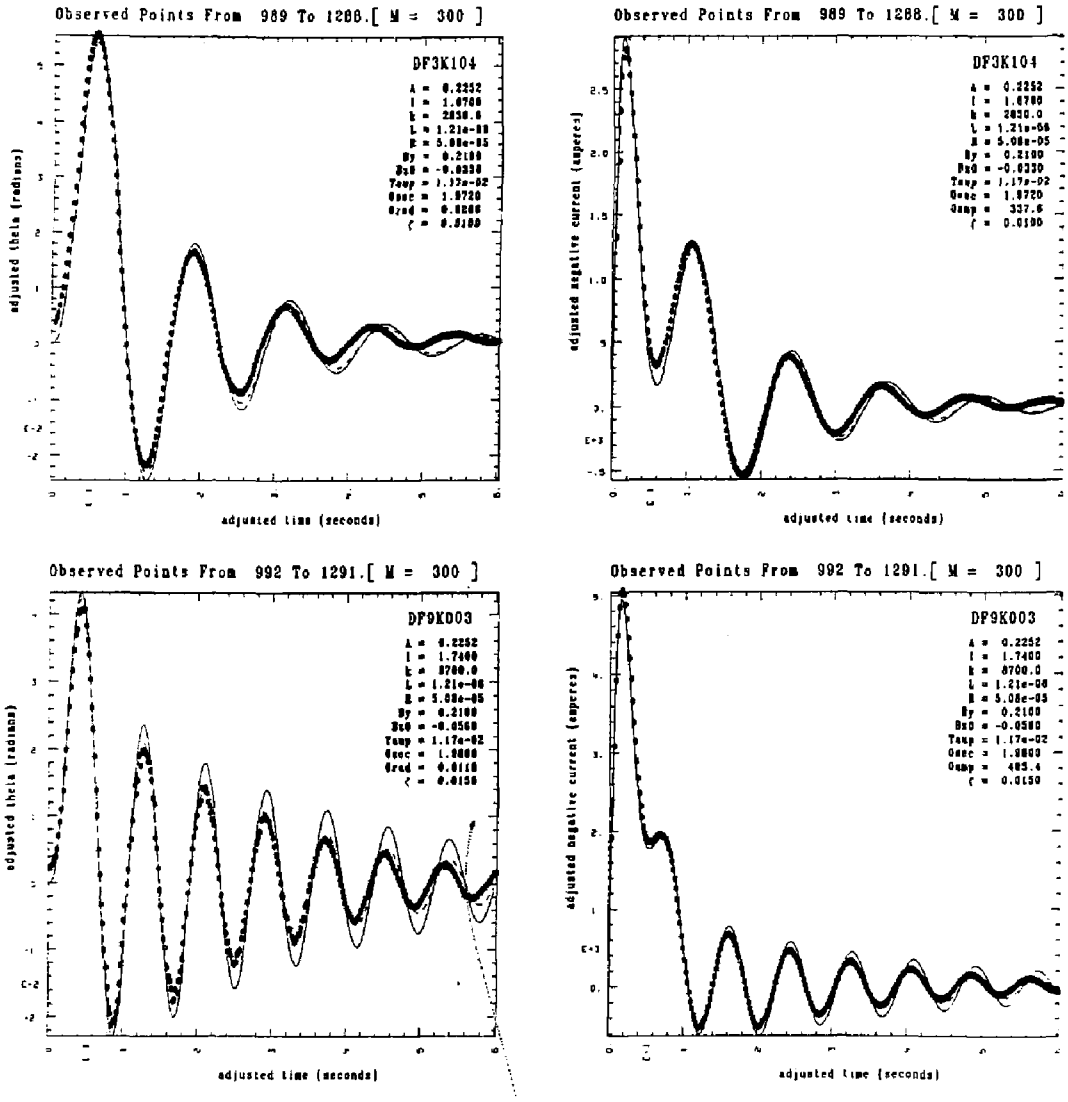

FIG. 11.

Combined Field Tests: Copper Loop.

Asterisks = observed data.
Dashed line = complete numerical solution including mechanical damping.
Solid line = simplified analytic solution.

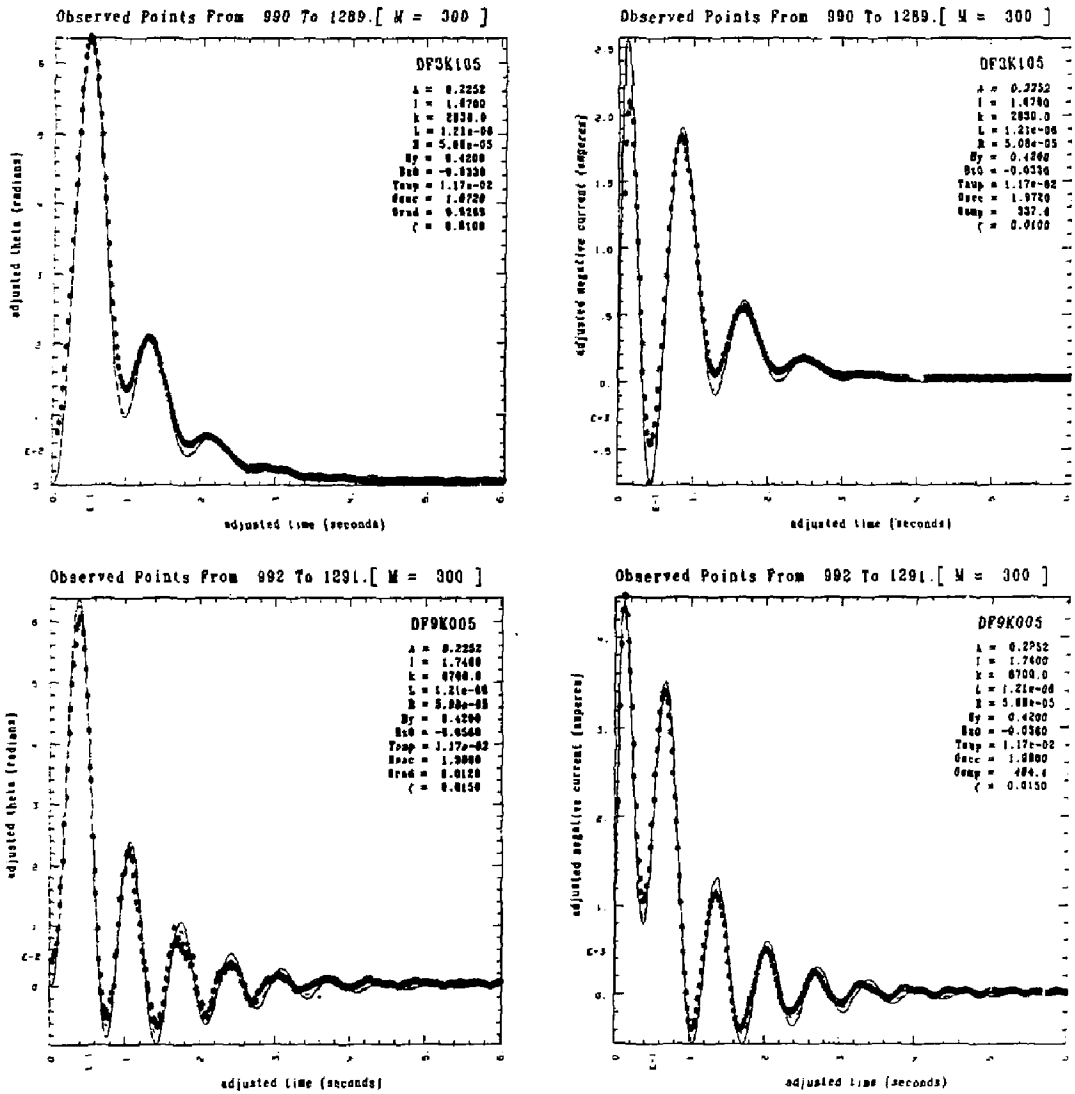

FIG. 12.

Combined Field Tests: Copper Loop.

Asterisks = observed data.
Dashed line = complete numerical solution *including mechanical damping.*
Solid line = simplified analytic solution.

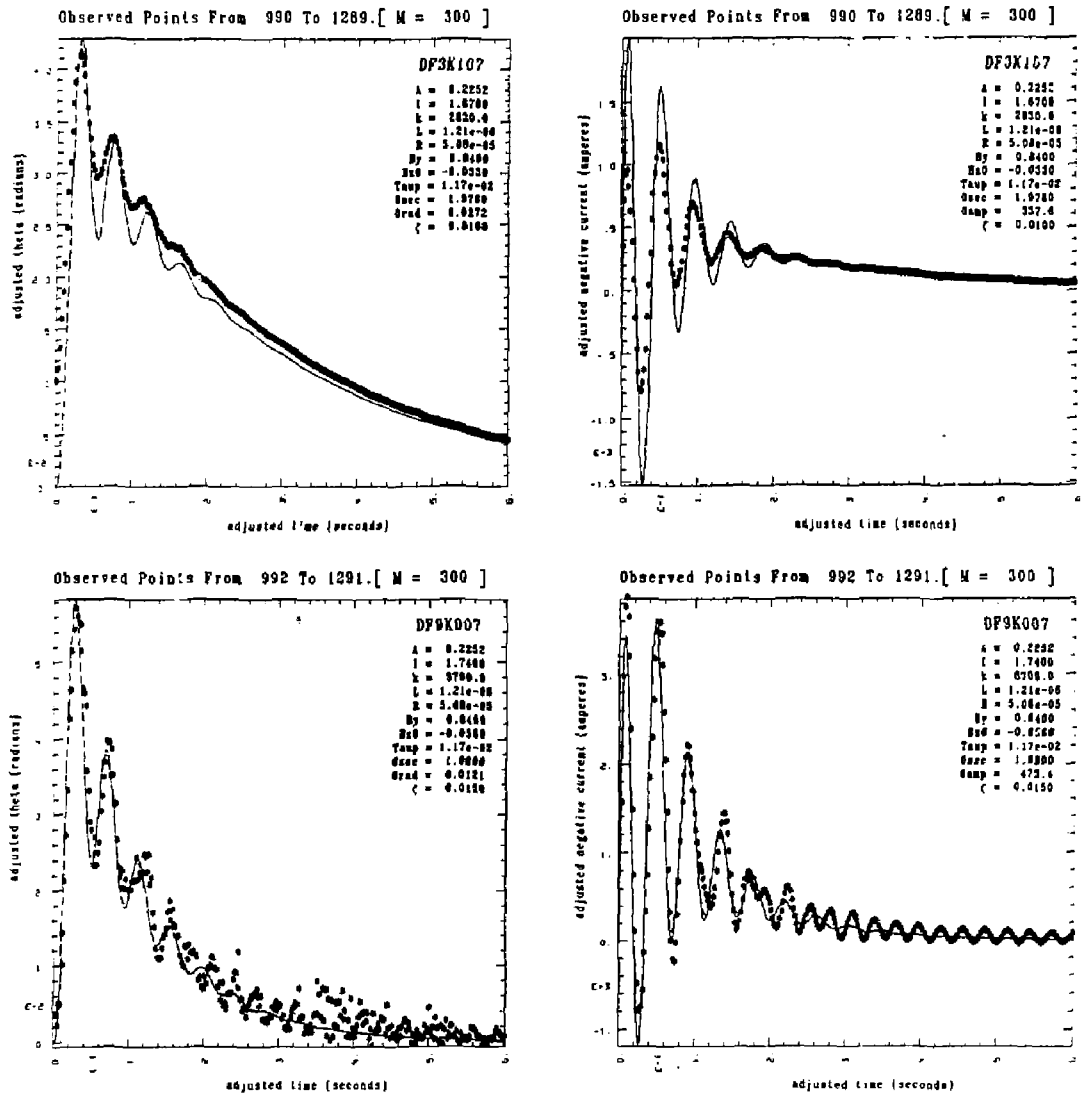

FIG. 13.

Combined Field Tests: Copper Loop.

Asterisks = observed data.
Dashed line = complete numerical solution including mechanical damping.
Solid line = simplified analytic solution.

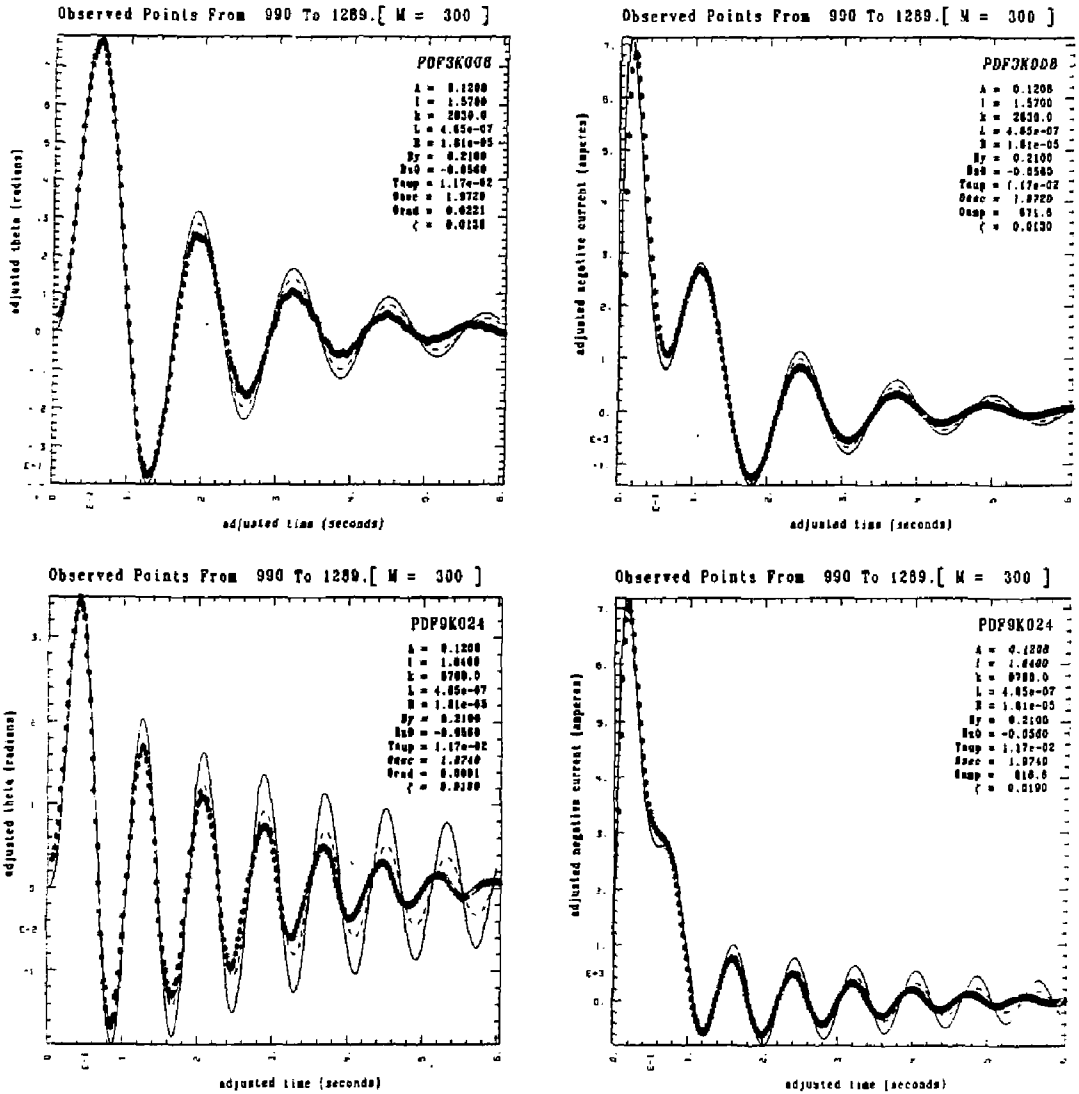

FIG. 14.

Combined Field Tests: Copper Plate.

Asterisks = observed data.
Dashed line = complete numerical solution including mechanical damping.
Solid line = simplified analytic solution.

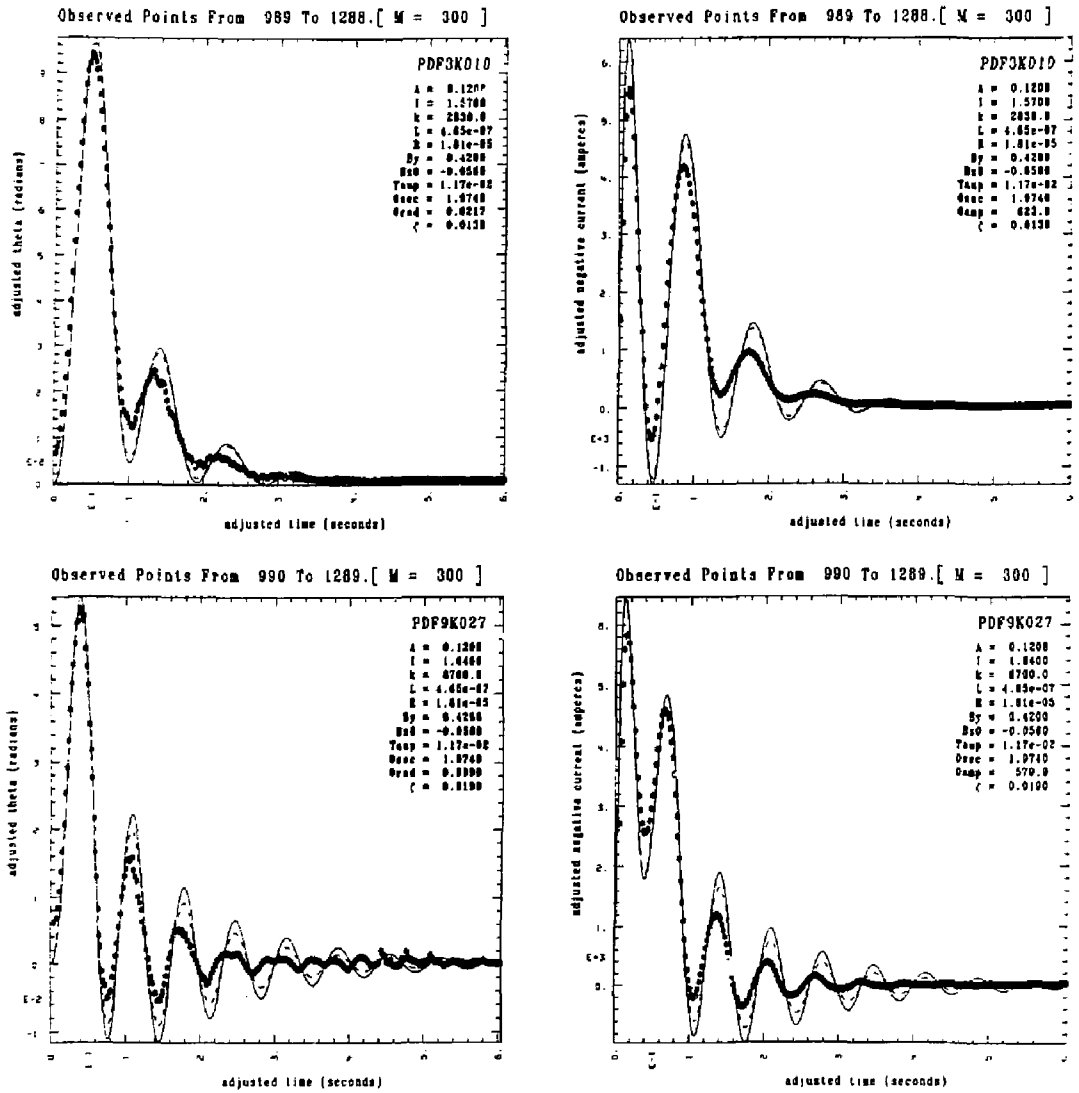

FIG. 15.

Combined Field Tests: Copper Plate.

Asterisks = observed data.
Dashed line = complete numerical solution including mechanical damping.
Solid line = simplified analytic solution.

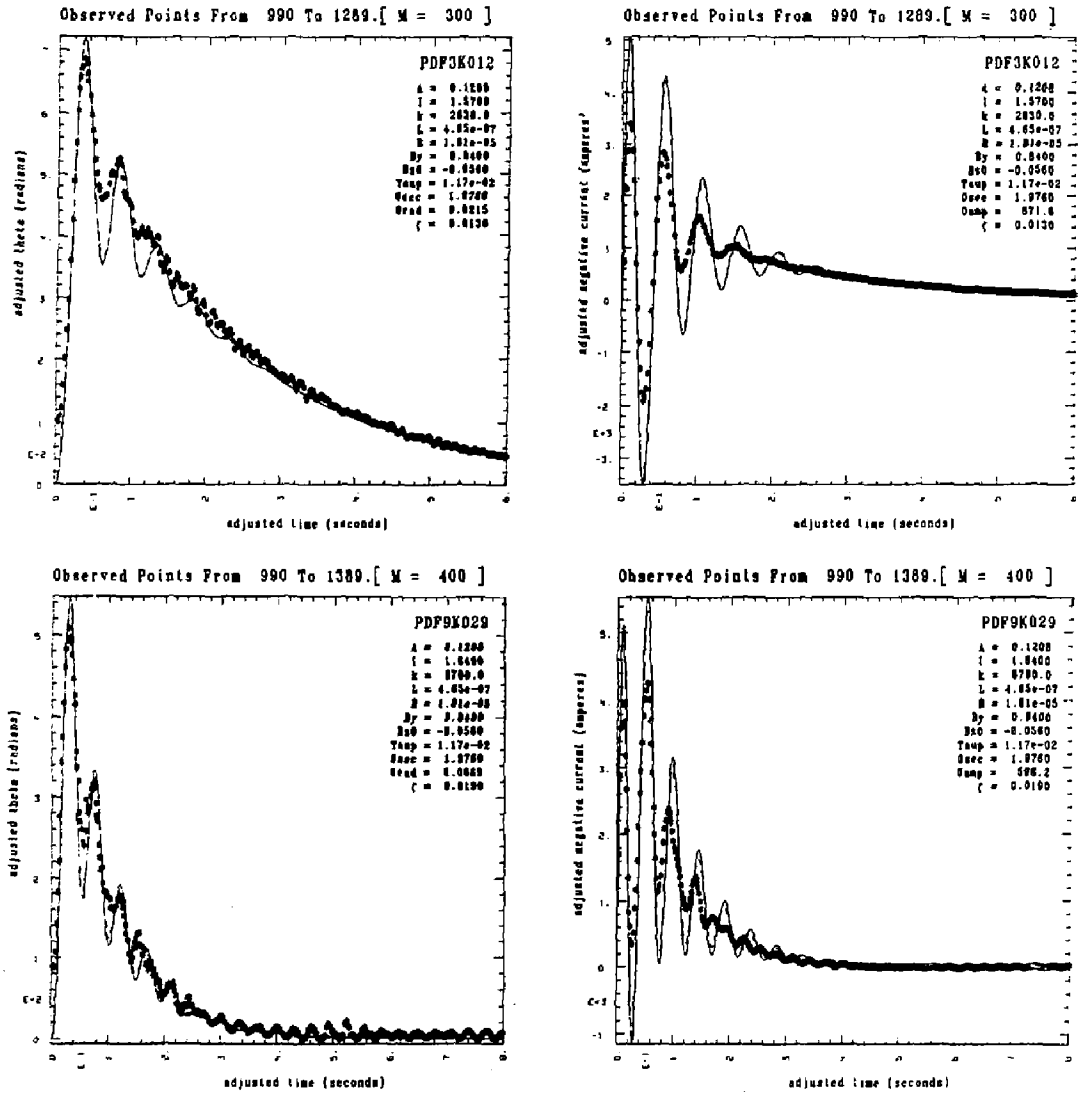

FIG. 16.

Combined Field Tests: Copper Plate.

Asterisks = observed data.
Dashed line = complete numerical solution
including mechanical damping.
Solid line = simplified analytic solution.

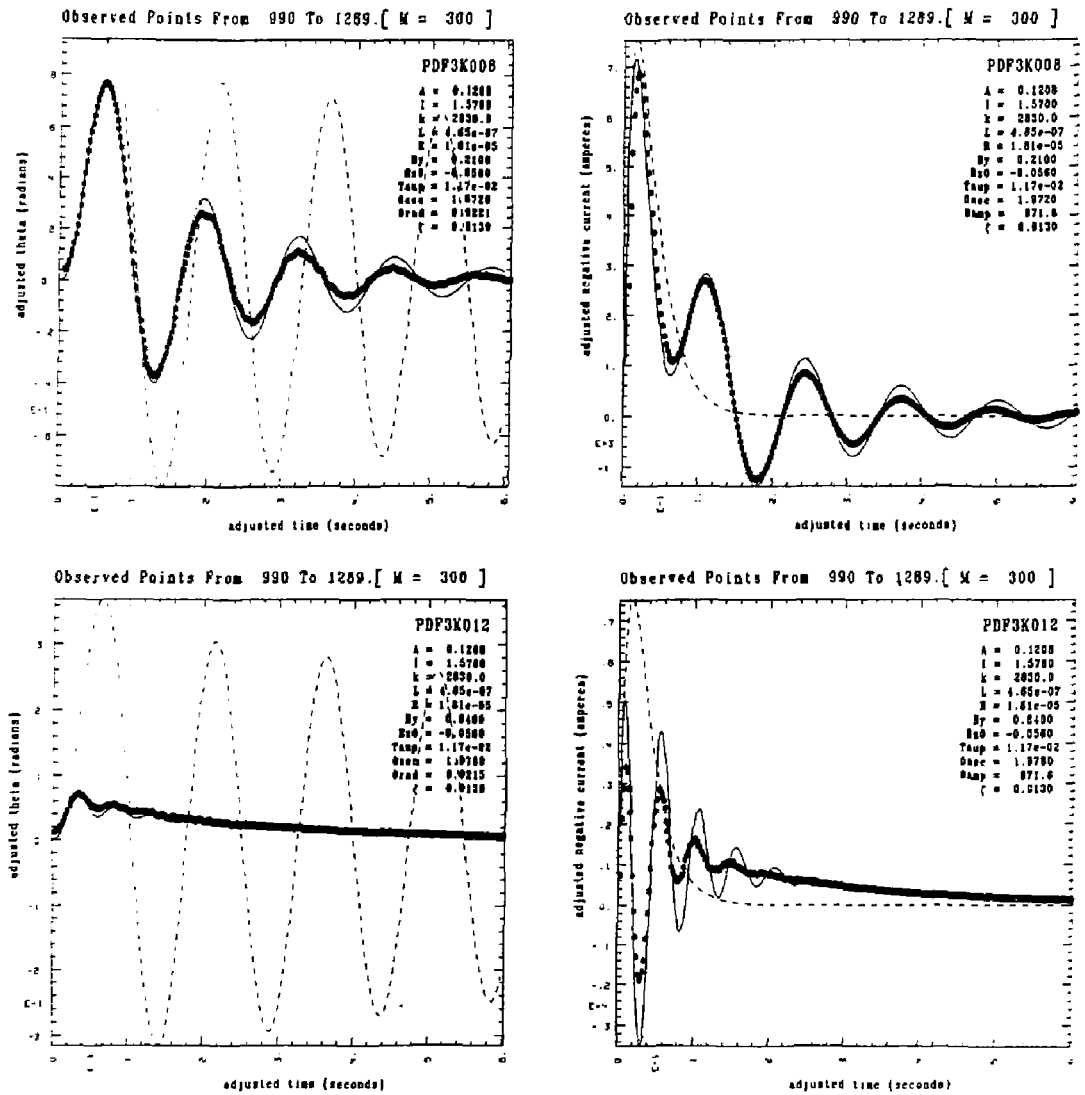

FIG. 17.

Combined Field Tests: Copper Plate.

Asterisks = observed data.
Dashed line = uncoupled numerical solution including mechanical damping.
Solid line = simplified analytic solution.

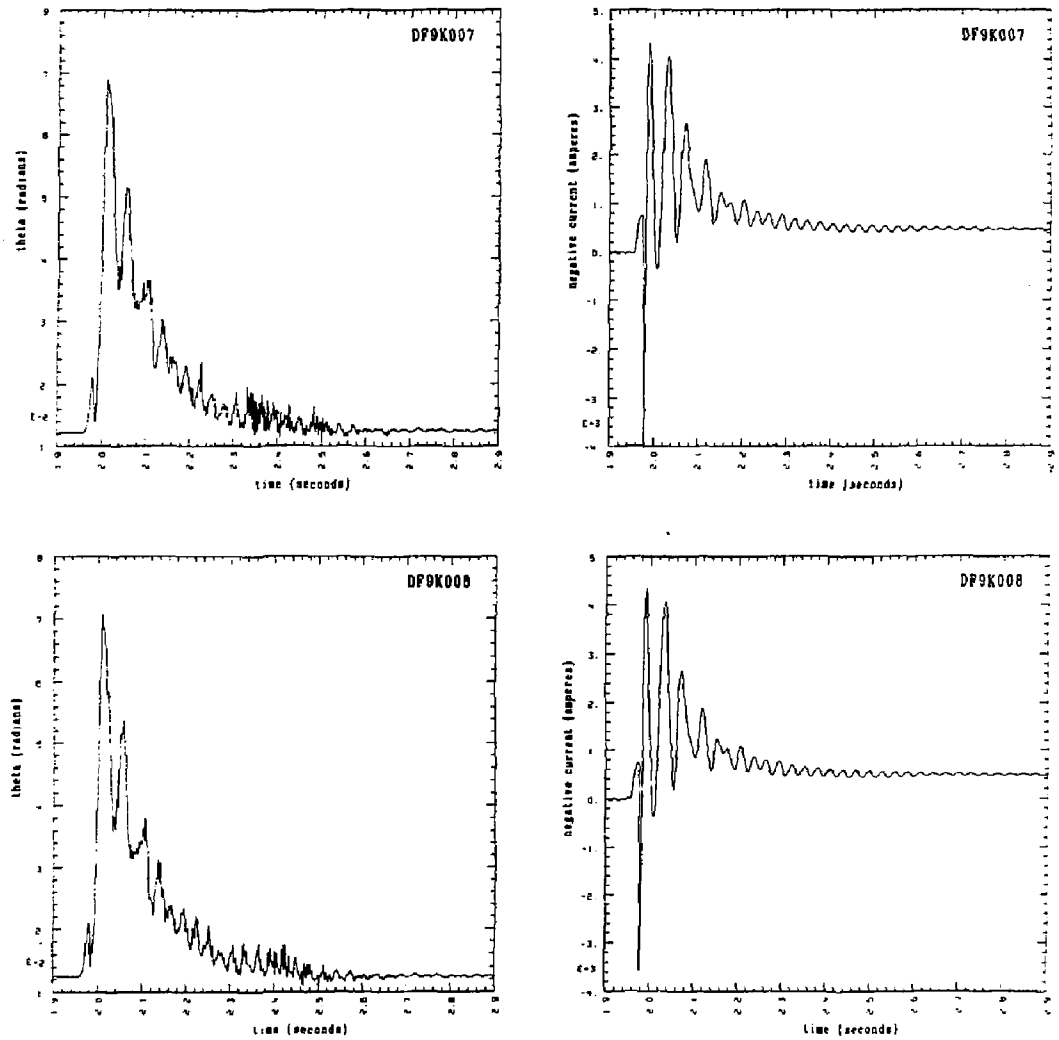

FIG. 18.

Combined Field Tests: Copper Loop.

Observed Data
Repeatability Illustration.

EXTERNAL DISTRIBUTION IN ADDITION TO TIC UC-20

Plasma Res Lab, Austre Nat'l Univ, AUSTRALIA
Dr. Frank J. Paoloni, Univ of Wollongong, AUSTRALIA
Prof. I.R. Jones, Flinders Univ., AUSTRALIA
Prof. M.H. Brennan, Univ Sydney, AUSTRALIA
Prof. F. Cap, Inst Theo Phys, AUSTRIA
Prof. Frank Verheest, Inst theoretische, BELGIUM
Dr. D. Palumbo, Dg XII Fusion Prog, BELGIUM
Ecole Royale Militaire, Lab de Phys Plasmas, BELGIUM
Dr. P.H. Sakanaka, Univ Estadual, BRAZIL
Dr. C.R. James, Univ of Alberta, CANADA
Prof. J. Teichmann, Univ of Montreal, CANADA
Dr. H.M. Skarsgard, Univ of Saskatchewan, CANADA
Prof. S.R. Sreenivasan, University of Calgary, CANADA
Prof. Tudor W. Johnston, INRS-Energie, CANADA
Dr. Hannes Barnard, Univ British Columbia, CANADA
Dr. M.P. Bachynski, MPB Technologies, Inc., CANADA
Zhengwu Li, SW Inst Physics, CHINA
Library, Tsing Hua University, CHINA
Librarian, Institute of Physics, CHINA
Inst Plasma Phys, Academia Sinica, CHINA
Dr. Peter Lukac, Komenskeho Univ, CZECHOSLOVAKIA
The Librarian, Culham Laboratory, ENGLAND
Prof. Schatzman, Observatoire de Nice, FRANCE
J. Radet, CEN-BP6, FRANCE
AM Dupas Library, AM Dupas Library, FRANCE
Dr. Tom Mual, Academy Bibliographic, HONG KONG
Preprint Library, Cent Res Inst Phys, HUNGARY
Dr. S.K. Trehan, Panjab University, INDIA
Dr. Indra, Mohan Lal Das, Banaras Hindu Univ, INDIA
Dr. L.K. Chavda, South Gujarat Univ, INDIA
Dr. R.K. Chhajlani, Var Ruchi Marg, INDIA
P. Kaw, Physical Research Lab, INDIA
Dr. Phillip Rosenau, Israel Inst Tech, ISRAEL
Prof. S. Cuperman, Tel Aviv University, ISRAEL
Prof. G. Rostagni, Univ Di Padova, ITALY
Librarian, Int'l Ctr Theo Phys, ITALY
Miss Ciella De Palo, Assoc EURATOM-CNEN, ITALY
Biblioteca, del CNR EURATOM, ITALY
Dr. H. Yamato, Toshiba Res & Dev, JAPAN
Prof. M. Yoshikawa, JAERI, Tokai Res Est, JAPAN
Prof. T. Uchida, University of Tokyo, JAPAN
Research Info Center, Nagoya University, JAPAN
Prof. Kyoji Nishikawa, Univ of Hiroshima, JAPAN
Prof. Sigeru Mori, JAERI, JAPAN
Library, Kyoto University, JAPAN
Prof. Ichiro Kawakami, Nihon Univ, JAPAN
Prof. Setoshi Itoh, Kyushu University, JAPAN
Tech Info Division, Korea Atomic Energy, KOREA
Dr. R. England, Civdad Universitaria, MEXICO
Bibliotheek, Fom-Inst Voor Plasma, NETHERLANDS
Prof. B.S. Liley, University of Waikato, NEW ZEALAND
Dr. Suresh C. Sharma, Univ of Calabar, NIGERIA
Prof. J.A.C. Cabral, Inst Superior Tech, PORTUGAL
Dr. Octavian Petrus, ALI CUZA University, ROMANIA
Prof. H.A. Hellberg, University of Natal, SO AFRICA
Dr. Johan de Villiers, Atomic Energy Bd, SO AFRICA
Fusion Div. Library, JEN, SPAIN
Prof. Hans Wilhelmson, Chalmers Univ Tech, SWEDEN
Dr. Lennart Stenflo, University of UMEA, SWEDEN
Library, Royal Inst Tech, SWEDEN
Dr. Erik T. Karlson, Uppsala Universitet, SWEDEN
Centre de Recherchesen, Ecole Polytech Fed, SWITZERLAND
Dr. W.L. Weise, Nat'l Bur Stand, USA
Dr. W.M. Stacey, Georg Inst Tech, USA
Dr. S.T. Wu, Univ Alabama, USA
Prof. Norman L. Oleson, Univ S Florida, USA
Dr. Benjamin Ma, Iowa State Univ, USA
Prof. Magne Kristiansen, Texas Tech Univ, USA
Dr. Raymond Askew, Auburn Univ, USA
Dr. V.T. Tolok, Kharkov Phys Tech Ins, USSR
Dr. D.D. Ryutov, Siberian Acad Sci, USSR
Dr. G.A. Eliseev, Kurchatov Institute, USSR
Dr. V.A. Glukhikh, Inst Electro-Physical, USSR
Institute Gen. Physics, USSR
Prof. T.J. Boyd, Univ College N Wales, WALES
Dr. K. Schindler, Ruhr Universitat, W. GERMANY
Nuclear Res Estab, Julich Ltd, W. GERMANY
Librarian, Max-Planck Institut, W. GERMANY
Dr. H.J. Kaeppler, University Stuttgart, W. GERMANY
Bibliothek, Inst Plasmaforschung, W. GERMANY